Petrology, Vol. 12, No. 1, 2004, pp. 17–36. Translated from Petrologiya, Vol. 12, No. 1, 2004, pp. 22–45.

Formation of Fluorine-Rich Magmas by Fluid Filtration through Silicic Magmas: Petrological and Geochemical Evidence of Metamagmatism

S. S. Abramov

Institute of Geology of Ore Deposits, Petrography, Mineralogy, and Geochemistry (IGEM), Russian Academy of Sciences, Staromonetnyi per. 35, Moscow, 119017 Russia; e-mail: abramov@igem.ru

Received January 19, 2003

Abstract—The composition of fluorine-rich silicic rocks from various geologic environments (differing in depth of formation, association, age, etc.) suggests that their differentiation is related to metamagmatism, fluid filtration through magmas. Retrograde magma boiling in a large magma chamber produces an increase in pressure. This results either in explosive ejection of melt on the surface or in passive chamber degassing (magma remains in place). In the latter case, fluid is filtered under temperature- and pressure-gradient conditions through magmas and rocks of the apical parts of magma chambers. This process causes the development of feldspar megablasts far from the contact and recrystallization of biotite with an increase in its iron and fluorine contents. Granophyre quartz–feldspars intergrowths and rapakivi textures form directly near the contact. The altered rocks are partially melted in the back zone of the metasomatic rocks giving rise to high-fluorine magmas. Modeling of the impact of metamagmatic fluids on magmas demonstrated that, when fluid rises and its temperature decreases, the solubility of HF decreases in fluid and increases in magma. High F contents in fluid result in the redistribution of elements between fluid and magma. Mg and LREE form stable soluble F complexes and are removed from the magma, whereas Fe, Mn, and HREE are retained in the melt. Prolonged filtration results in the formation of iron-rich magmas enriched in HREE. If oxygen fugacity in the magmatic source of fluid is higher than QFM +1...+2, fluid filtration leads to the formation of high-fluorine oxidized melts, whereas, if the initial oxygen fugacity is lower than QFM +1...+2, more reduced high-fluorine melts are produced. Modeling of the dynamics of heat and mass transfer showed that an open degassed magmatic system develops through several stages: (1) formation of a cupola of fully or partially crystallized granite at the roof of the massif and beginning of eutectic magma crystallization in the central part of the chamber; (2) fluid filtration (2–500 years) under temperature-gradient conditions produces fluorine-rich magmas with continuously increasing contents of fluorine and related elements in the upper part of the cupola; (3) in 5000–10000 y the conducting body is heated up to the temperature of the central part of the chamber; then, either F and related components are removed into the upper cooled part or such magmas are removed as dikes of ongonite or topaz rhyolite and ignimbrite; and (4) when degassing is terminated in the main chamber, fluorine-rich magmas begin to crystallize in the cupola and peculiar ore-bearing silicic magmas are generated.

INTRODUCTION

Studies of ore-bearing granitoids from various regions suggest that, among the factors characterizing the crystallization conditions of productive magmas, oxygen activity and halogen concentrations in magmas are the main controls on the type of mineralization (Huspeni *et al.*, 1984; Ryabchikov *et al.*, 1976; Ague and Brimhall, 1988; Blevin and Chappell, 1992, 1995; Borisenko *et al.*, 1996; Abramov and Borisovskiĭ, 1996). The partition coefficients of Mo, W, Cu, and Sn between melt and crystals change depending on f_{O_2}, which defines eventually which ore element will be removed from the magma (Candela, 1992; Candela and Piccoli, 1995). Burt *et al.* (1982) and other authors (e.g., Ague and Brimhall, 1988; Blevin and Chappell, 1992) argued that fluorine-rich granitoid magmas are relatively reduced. This conclusion was based on the occurrence of iron-rich mica (or, occasionally, another Fe–Mg silicate) and magnetite as a typical assemblage of fluorine-rich granitoids. Recent estimates of the redox conditions of fluorine-rich magmas (Stix and Gorton, 1990; Nash, 1993; Rieder *et al.*, 1996; Abramov and Rasskazov, 1997) suggested that their crystallization may occur in a wide range of oxygen fugacity between QFM and HM. This is difficult to explain if these magmas are regarded as products of melting of reduced sediments (Ague and Brimhall, 1988) or mantle rocks (Frost and Frost, 1997).

As the Sm–Nd and Rb–Sr isotopic data (Kovalenko *et al.*, 1999) indicate that rare-metal granitoids developed in isotopically closed magma reservoirs, the genesis of high-fluorine silicic rocks (HFSR) has to be related to the processes of chamber differentiation including crystal fractionation and/or fluid–magma interaction.

The efficiency of the process of crystallization differentiation is limited in silicic magmas by their high viscosity. Sparks *et al.* (1984) demonstrated that the very high viscosity of silicic melts prevents crystal removal from its birthplace. This mechanism can operate efficiently, if the viscosity of the melt will be reduced, which, according to the experiments of Dingwell *et al.* (1985), requires an HF concentration of up to 3 wt %. Such fluorine concentrations were detected in strongly differentiated ore-bearing silicic melts (Webster and Duffield, 1994), i.e., in evolved rather than in initial melts. Kovalenko and Kovalenko (1982) supposed that the enrichment of acid systems in fluorine, rubidium, and other elements occurred in two stages. Initially, the mechanism of fractional crystallization operated in intermediate and moderately acid melts, and the magma was preliminarily enriched in incompatible components. The subsequent development of ore-bearing magmas resulted from the fluid-assisted redistribution of components. Fluid differentiation during magma crystallization is related to the appearance of a fluid phase owing to retrograde magma boiling under isobaric conditions (Eichelberger *et al.*, 1986; Tait *et al.*, 1989). The plausibility of such a scheme for the evolution of a magmatic system with HFSR is supported by the results of melt inclusion studies (Naumov *et al.*, 1993; Stix and Gorton, 1990; Webster and Duffiel, 1994; Lowenstern, 1994) and oxygen and hydrogen isotope systematics of rocks (Taylor *et al.*, 1983). Based on our own and published data, a model is developed in this paper for the fluid influence on silicic magmas (metamagmatism after Korzhinskiĭ, 1973), which allows us to explain the observed scatter of estimates of oxygen fugacity, variations in bulk compositions, and geochemical signatures of fluorine-rich granitoids.

GENERAL GEOLOGIC POSITION OF HFSR

High-fluorine silicic rocks compose a broad group of silicic rocks formed in the hypabyssal (lithium–fluorine granites, metaluminous fluorine granites, and late phases of rapakivi granites) and subvolcanic facies as small intrusive bodies (ongonite and ongorhyolite) or extrusive complexes (topaz rhyolite, tuffs, and ignimbrites). Detailed descriptions of particular systems were presented by Shcherba (1960), Kovalenko and Kovalenko (1976), Burt *et al.* (1982), and others. There are several features of HFSR that are obviously in conflict with the traditional view of their formation from residual magmas:

(1) transition from weakly differentiated to strongly differentiated granitoids within a single massif, pluton, or volcanic edifice;

(2) low degrees of HFSR crystallinity in the volcanic and subvolcanic facies; and

(3) active character of HFSR contacts with consolidated rocks.

Transitions from Weakly Differentiated to Strongly Differentiated HFSR

In the Long Valley system, Hildreth (1979) and Mahood and Hildreth (1983) reported an eruption sequence from early low-temperature Bishop Tuff rhyolites (720°C) to higher temperature rocks (790°C). The early and late rocks have fundamentally different geochemical signatures: the early rhyolites are rich in Rb, U, HREE, F, and Cl; whereas the late rocks are high in Ba, Sr, and Zr. According to the *Ilm-Mag* oxygen barometer, oxygen fugacity increased in the late rhyolites by 0.9 logarithmic units. According to petrological analysis, crystal fractionation and assimilation played a minor role in the formation of this series (Davies and Halliday, 1998), and, consequently, only component redistribution by fluid transfer could be of prime importance.

In the Cerro Toledo complex of ultrasilicic fluorine-rich rocks, Stix and Gorton (1990) and Stix and Layne (1996) established that the degree of differentiation increases from the bottom toward the roof of a pyroclastic sequence. The concentrations of F, Cl, Nb, Cs, and B increase regularly in melt inclusions from the sequential portions of pyroclastic rocks. According to Stix and Layne (1996), this reflects the dynamics of progressive enrichment of the apical part of the parent magma chamber as a result of fluid influence on these magmas. Water concentration is constant in the melt inclusions. According to the *Ilm–Mag* oxygen barometer, oxygen fugacity decreased by approximately one order of magnitude, and relatively reduced (QFM – 1) halogen-rich magmas formed during the final stages of evolution.

In the Honeycomb Hills system (Congdon and Nash, 1988, 1991; Nash, 1993), upper (topaz rhyolite tuffs) and lower (subvolcanic cupola of topaz rhyolite) parts have been investigated. The composition of biotite from extrusive rocks indicated an increase in fluorine content upward in the section, but the maximum fluorine concentrations were attained in the rocks of the subvolcanic cupola as a result of the maximum degree of differentiation of its magmas. This system is of special interest, because of the finding of biotite with presumably the highest fluorine contents among the published analyses (X_F = 70–90 mol %). This biotite is a 99% siderophyllite–annite solid solution with respect to its Fe, Mg, and Al relationships. Oxygen fugacity was estimated from the Fe^{2+}/Fe^{3+} ratio of rhyolite glasses as QFM + 3.

Numerous examples of a gradual transition from ordinary unmineralized granites to HFSR are provided by hypabyssal complexes, which have been described in the classic reviews of the geology of granite-related deposits (Shcherba, 1960; Rundkvist *et al.*, 1971; Beskin *et al.*, 1979). Rub *et al.* (1999) demonstrated recently the complete identity of vertical zoning in two rare-metal massifs: Pogranichnyi (Russia) and Cinovec (Czech Republic). In both cases, a transition from

weakly differentiated to productive varieties was observed in the apical parts of the massifs within a distance of about 1.5 km. In the Katpar massif (central Kazakhstan), Abramov and Borisovskiĭ (1996) showed that mineralized and unmineralized granites compose a single massif. The mineralized types of granitoids represent the apical tubular part of this massif, and unmineralized weakly differentiated granites compose the inner portions of the intrusion (Orlov, 1990). The evolution of the pluton from early monzonite to unmineralized granitoids was accompanied by an increase in oxygen fugacity from initial QFM + 0.5 to QFM + 3. The formation of ore-bearing high-fluorine granitoids in the cupola of the magma chamber occurred under relatively reduced conditions (QFM + 1) (Abramov and Borisovskiĭ, 1996). These examples suggest that HFSR formation is related to the differentiation processes of ordinary magmas in the apical parts of magma chambers.

High Temperatures and Low Degrees of Differentiation of HFSR

The available data on the compositions and temperatures of entrapment of melt inclusion are indicative of a wide temperature range of HFSR formation, 540–1100°C (Naumov *et al.*, 1997; Koval' and Prokof'ev, 1998). According to Koval' and Prokof'ev (1998), such a wide temperature range for the formation of rare-metal granitoids is in conflict with the concept of HFSR development as a product of differentiation of residual low-temperature magmas. The scheme of gradual accumulation of incompatible elements in residual magmas is often disturbed. For instance, Webster and Duffield (1994) noted that the fluorine richest Taylor Creek rhyolites were formed at lower degrees of differentiation than low-fluorine varieties. The phenocrysts/groundmass ratio varies within 5–40% in the majority of subvolcanic HFSR studied (Kovalenko and Kovalenko, 1976; Burt *et al.*, 1982; Macdonald *et al.*, 1992), which is indicative of their origin at low degrees of crystallization. In the Honeycomb Hills system (Nash, 1993), the highest fluorine rhyolites are not related to chamber differentiation and were formed in the vent facies, where crystallization differentiation could not be of much significance.

Interaction of Fluidized Magmas with Consolidated Rocks

The existence of zones affected by fluids from high-fluorine magmas in previously consolidated granitoids is a striking feature of the structure of HFSR massifs indicating their high-temperature character. Such an active interaction was first presented in the classic descriptions of the granitoid intrusions of central Kazakhstan: Karkaralinskiĭ, Ortau, and Bayan Aula (Dmitrievskiĭ, 1952; Anikeeva, 1968; Monich, 1957; Buzkova, 1989). Such zones of fluid impact were studied in detail in the contact aureoles of the Murzatai and Katpar massifs, Central Kazakhstan (Abramov and Borisovskiĭ, 1996). A remarkable characteristic of these alterations is their strict confinement to highly permeable biotite granites and granodiorites, whereas massive hornfels are almost unaffected. The influence of leucogranite magmas on rocks is manifested by the intrusion of dike swarms and simultaneous development of fields of metasomatic alteration. Initial changes (50–300 m from the contact) include an increase in the albite mole fraction of plagioclase (from $An_{15–20}$ to $An_{8.5}$), an increase in iron (from $Bt_{35–39}$ to Bt_{54}) and fluorine contents of biotite, and development of *Kfs* megablasts ($Ort_{80–90}Ab_{20–10}$). The degree of alteration of biotite granites increases toward the leucogranite bodies. This is recorded in the disappearance of typical granite textures and formation of rock areas with extensive development of sodic plagioclase as rims and fringes replacing the *Pl* of initial rocks. There is a concomitant increase in the abundance of reaction *Kfs* megablasts ($Ort_{90}Ab_{10}$, transitional microcline), which replace the newly formed sodic plagioclase of altered rocks.

The maximum alterations were observed in the contact zone (50–0 m), where the amount of plagioclase declines and its anorthite mole fraction increases up to An_{19}. The newly formed *Kfs* of this zone is represented by small grains (in contrast to megablasts) and is compositionally close to anorthoclase, $Ort_{43.9}Ab_{48.9}An_{7.2}$. In addition, areas with granophyre textures appear in the rocks as thin graphic and subgraphic intergrowths of *Qtz* and alkali feldspar with the composition $Ort_{69}Ab_{31}$–$Ort_{50}Ab_{50}$. The occurrence of areas with granophyre fabrics in the rocks is indicative of partial melting, because similar granophyre textures are typical of the fine-grained groundmass of the parental HFSR. The investigation of the cryptic zoning of feldspars in the zones of such quartz–feldspar intergrowths (Lipman *et al.*, 1997) demonstrated that the granophyres are products of rapid melt crystallization under undercooling caused by the decompression of a magma chamber. A similar interpretation was proposed by Price *et al.* (1996).

Temperature estimates for the altered rocks of the aureole by a number of geothermometers (Abramov and Borisovskiĭ, 1996) suggest a very high temperature gradient from 450–500°C in the outer altered zone (300–400 m from the contact) to 770–800°C in the zone of direct contact of magma with partially molten metasomatic rocks, which could be indicative of the short duration of the processes that caused metasomatism and melting. This is indirectly supported by the absence of distinct zoning in the alteration aureole: associations characteristic of the outer parts of aureoles (megablasts of *Kfs* + *Ab*) occur in other zones up to direct contact with leucogranites. Megablasts corroded by granophyre aggregates were documented in the areas of granophyre development. Such *Kfs* grains are

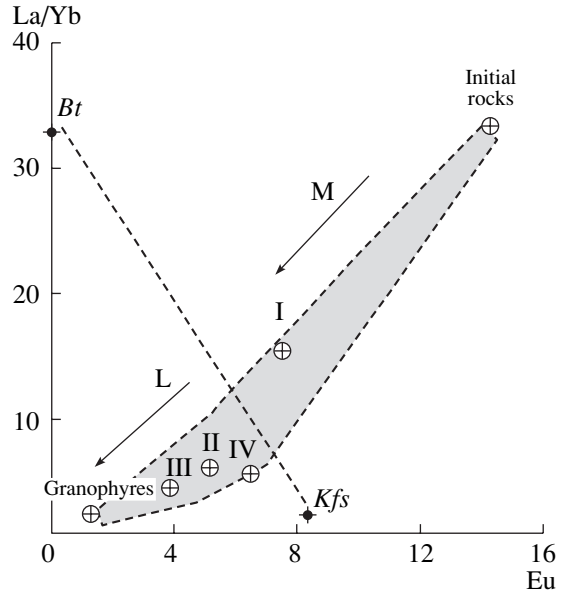

Fig. 1. Geochemical variations in altered roof rocks (initial rocks are biotite granites) under the influence of fluids from high-fluorine magmas. I–IV are the sequential zones of alteration: I, outer zone of the aureole, 300 m from the contact; II, III, and IV, metasomatic rocks formed at distances of 6, 2, and 1 m from the contact, respectively; the initial data are after Abramov and Borisovskiĭ (1996). Chondrite-normalized concentration ratios are shown along the *y* axis, and chondrite-normalized REE concentrations, along the *x* axis.

mantled by sodic plagioclase ($An_{10–12}$), which is similar in composition to the plagioclase of the parental leucogranites, and the rocks acquire the appearance of porphyritic rapakivi granites with a fine-grained quartz–plagioclase–biotite groundmass and *Kfs* and *Qtz* phenocrysts. Thus, the reason for the formation of the rapakivi texture in the hybrid contact rocks is the rapid movement of the front of alteration and temperature.

Toward the contact the REE spectra of altered rocks approach those of the parental ore-bearing HFSR. Figure 1 shows an REE variation trend for altered rocks after the data of Abramov and Borisovskiĭ (1996). The metasomatic crystallization of *Kfs* and *Bt* in the contact rocks must result in a gradual decrease in La/Yb ratio and europium content. Completely altered rocks must straddle the *Bt–Kfs* line (Fig. 1). However, metasomatic rocks from the zones of sequential alteration (II–III–IV) show much lower La/Yb and Eu*/Eu values than is expected for the development of these two metasomatic minerals and are related, as follows from Fig. 1, to granophyre formation. Thus, the trend initial rock–I corresponds to the metasomatic alteration of wallrocks, and trend II–IV corresponds to the progressively increasing partial melting of altered rocks.

Such zones of intense reworking of the consolidated granitoids of early intrusive phases by leucocratic granite intrusions are widespread and have been described in many ore provinces (Pitfield *et al.*, 1990; Linnen and Williams-Jones, 1995). Of special importance is the example of HFSR interaction with wallrocks in the Crater Lake volcanic system (Bacon, 1992; Sisson and Bacon, 1999). Blocks of granodiorite, diabase, diorite, and other intrusive rocks occur in the products of the caldera-forming Mount Mazama eruption. Xenoliths experienced partial melting owing to interaction with silicic magmas at the magma chamber level (3–4 kbar). The primary assemblages of granodiorite xenoliths include *Pl*, *Opx*, *Aug*, *Mag*, *Ilm*, *Ap*, and *Zrn* and late *Qtz*, *Hbl*, *Bt*, and *Kfs*. The process of melting was accompanied by the replacement of the *Hbl* + *Aug* + *Bt* + *Qtz* association by the *Opx* + *Mag* + *Ilm* aggregate, and, depending on the degree of melting, the xenoliths contain residual phases, newly formed minerals, and glass in varying proportions. The composition of glass is identical in all xenolith types and corresponds to rhyolite (75–77 wt % SiO_2). The fluorine and chlorine contents of glasses increase with increasing degree of xenolith melting, which is recorded in the composition of recrystallized biotite, whose fluorine and chlorine concentrations increase from 1 to 5 wt % and from 0.1 to 0.25 wt %, respectively. The geochemical transformations of melting products include Rb, Th, Cs, and Y enrichment. The concentrations of REE, except for Eu, increase in the partially molten varieties relative to the initial rocks. Thus, the geologic situation is reminiscent of magma interaction with the consolidated roof rocks of hypabyssal granitic plutons. In both cases, the same changes in bulk compositions and geochemical characteristics were observed. However, these blocks retained all the stages of partial melting, because they were rapidly conveyed to the surface during the eruption.

The isotopic and geochemical investigations of the Taylor Creek HFSR by Wittke *et al.* (1996) also suggested a contribution from the processes of roof rock assimilation to the genesis of high-fluorine melts. The zone of hybridized rocks is situated near the intrusion roof and extends into the central parts to a depth of 300 m. It was formed shortly before the volcanic discharge. Magma hybridization resulted in isotopic disequilibrium between phenocrysts and groundmass formed during the melting of the roof rocks and appearance of biotite among HFSR minerals. Despite the process of wallrock assimilation by magma, oxygen fugacity remained near the QFM buffer both in hybridized and nonhybridized varieties (Wittke *et al.*, 1996).

These examples of melting of contact rocks under the influence of silicic magmas show similar scenarios of their development: formation of metasomatic rocks of a magmatic stage, derivation of a magma of stable composition independent on the initial source composition, and constant intensive parameters of the melting process (f_{O_2} and f_{HF}). All these features point to the process of magmatic replacement produced by intense

Petrological and geochemical characteristics of HFSR

System	Composition, phenocrysts	F content, wt %	Ce/Yb, Eu/Eu*	Oxygen fugacity, method of estimation	Crystallization temperature, °C	Reference
Honeycomb Hills, Utah; 4.7 Ma	Rhyolites; *Qtz*, *Bt*, *Pl*, *Kfs*, *Toz*, *Mag*	0.8–2.5	4.9, 0.05	Higher than NNO; Fe^{2+}/Fe^{3+} in glass	600	(Nash, 1993)
Cerro Toledo, New Mexico; 1.45 Ma	Rhyolites; *Qtz*, *Kfs*, *Pl*, *Hbl*, *Bt*, *Mag*, ±*Opx*, ±*Fa*	0.11	14.7, 0.07	QFM + 0.5; *Ilm–Mag* oxygen barometer	700–813	(Stix, Gorton, 1990)
Toano Range, Nevada; 12.9 Ma	Rhyolites; *Qtz*, *Kfs*, *Pl*, *Fa*, *Bt*, *Toz*, *Mag*	0.24	5.03, 0.02	QFM; *Fa* + *Mag* + *Qtz* association		(Price *et al*., 1992)
Katpar, Kazakhstan; 300 Ma	Leucogranites; *Qtz*, *Pl*, *Kfs*, *Bt*, *Mag*, *Ilm*, *Flu*	0.1	6.02, 0.06	QFM + 1; *Kfs–Bt–Mag* equilibria	750–800	(Abramov, 1996)
Bishop Tuffs, California; 0.7 Ma	Rhyolite tuffs; *Qtz*, *Opx*, *Cpx*, *Bt*, *Mag*, *Ilm*	0.08	15, 0.03	QFM + 1.5; *Ilm–Mag* oxygen barometer	780	(Mahood, Hildreth, 1983)
Taylor Creek, New Mexico; Tertiary	Rhyolites; *Qtz*, *Pl*, *Kfs*, *Bt*, *Hbl*	3.0		QFM + 0.4; *Ilm–Mag* oxygen barometer	798–800	(Webster, Duffield, 1994)
Spur Mountain	Rhyolites; *Qtz*, *Kfs*, *Pl*, *Bt*, *Toz*, *Fa*, *Mag*	0.7–1.25	8.1, 0.01	Near QFM; *Kfs–Bt–Mag* equilibrium	750–980	(Tsareva *et al*., 1991)
Vyborg rapakivi granite massif, Finland	Granites; *Qtz*, *Pl*, *Kfs*, *Bt*, *Mu*, *Mag*, *Hbl*, *Flu*, *Toz*			NNO–HM; Fe^{2+}/Fe^{3+} in mica	570–600	(Rieder *et al*., 1996)

fluid flow from the magma to the wallrocks as the main mechanism of melting.

Summing up the geological evidence, note that the choice of objects for investigations requires a certain dualism. On the one hand, subvolcanic and volcanic complexes provide an insight into the intensive parameters in the crystallization chamber owing to the preservation of phenocrysts, but are morphologically produced by processes occurring after the generation of fluorine-rich melts. On the other hand, hypabyssal HFSR are strongly altered and are less informative for the estimation of parameters, but they provide a good portrait of the magmatic apparatus that produced fluorine-rich magmas.

The data on the hypabyssal facies suggest that fluorine-rich magmas are formed in the apical parts of magma chambers, and the degree of rock differentiation increases upward. The geological and geophysical estimates of the apical cupola structures made up of HFSR were obtained by Lishnevskiĭ (1988, 1996). He showed that cupolas are confined to those portions of plutons where the maximum thickness of intrusive bodies was detected. The vertical size of the cupolas is up to 0.5–1.0 km, and their lateral extension is up to a few hundreds of meters. At the moment of fluorine-rich magma generation, the volume fraction of HFSR in the intrusive chamber is only a few hundredths of percent.

The crystallization temperatures of subvolcanic and volcanic HFSR varied (Table 1) from near eutectic (Honeycomb Hills, 600–670°C) to cotectic (Taylor Creek, 800°C; Cerro Toledo, 813°C; and Spur Mountain, 980°C). The sequence of magma appearance on the surface may be different, either from less differentiated to more differentiated (Cerro Toledo) or from more differentiated to less differentiated (Bishop Tuff). Nevertheless, the character of zoning in well-preserved subvolcanic structures (Honeycomb Hills) is suggestive of an increase in the degree of differentiation in the upper portions of subvolcanic bodies (necks and stock conduits). Both hypabyssal and subvolcanic structures bear evidence for the high-temperature fluid influence of magmas on the wallrocks, which was accompanied by metasomatic alterations, wallrock melting, and magma hybridization.

Thus, high-fluorine melts are generated in the upper cupola parts of magma chambers within a wide temperature range. This indicates a multistage prolonged origin of HFSR, and any model of HFSR formation must explain the temperature evolution of magmas and the occurrence of active contacts between the magma chamber and wallrocks.

CHARACTERISTICS OF THE BULK COMPOSITION AND GEOCHEMISTRY OF HFSR

Additional constraints for the construction of such an evolutionary model can be obtained from the analysis of variations in the bulk composition of HFSR. HFSR differ petrochemically from ordinary granites in higher alumina and lower silica contents (Kovalenko, 1979; Kovalenko and Kovalenko, 1982). In some cases, the differentiation process is accompanied by distinct

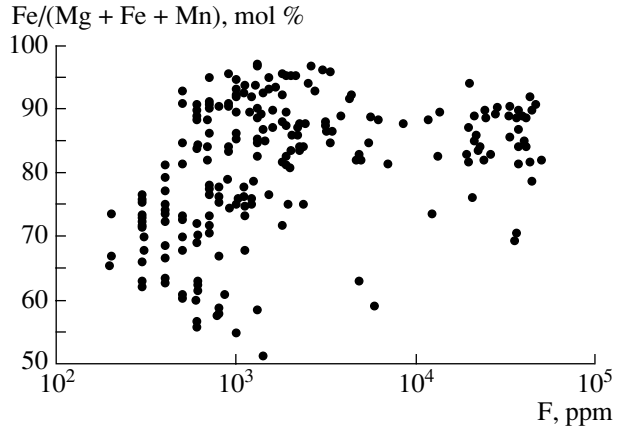

Fig. 2. Correlation of Fe/(Fe + Mg + Mn), mol %, and fluorine content (ppm) in fresh volcanic and subvolcanic silicic rocks. The data are after Kovalenko and Kovalenko (1976); Macdonald *et al.* (1992); Stix and Gorton (1990); Webster (1990); Nash (1993); Burt *et al.* (1982); Tsareva *et al.* (1991); and Naumov *et al.* (1997).

sodium accumulation in the melts (Kovalenko, 1979; Kuznetsov and Épel'baum, 1985; Webster and Duffield, 1994; Swanson *et al.*, 1988). Our analysis of compositional variations in a considerable number of HFSR complexes suggests that this correlation is not ubiquitous, which was also noted by Kovalenko (1976). A remarkable feature of HFSR composition is the strong correlation of iron and manganese contents (Burt *et al.*, 1982; Ague and Brimhall, 1988; Zaraiskii *et al.*, 1994; Abramov and Borisovskiĭ, 1996) with fluorine (Fig. 2). Figure 2 presents 254 analyses of young glassy subvolcanic HFSR from North America and Mongolia. A slight decrease in the Fe/(Fe + Mg + Mn) ratio of rocks at high fluorine content (>3000 ppm) is related to an increase in Mn/(Fe + Mg + Mn), which may be as high as 10–25 mol %. As the concentration of magnesium oxide in all HFSR is lower than 0.1 wt %, an increase in the Fe/(Fe + Mg + Mn) ratio of HFSR can be related to a decrease in magnesium content rather than iron accumulation.

Geochemical Characteristics of HFSR

Geochemical characteristics are used as a basis in many classification schemes for granitoids (Tauson, 1977). Comprehensive studies revealed several stable end-members and a complete spectrum of transitional varieties between them. Recent work has shown a wide occurrence of granitoids with high concentrations of phosphorus-bearing accessory minerals (apatite, monazite, etc.) (London *et al.*, 1998; Chnagshi *et al.*, 1998). Stix and Layne (1996), and Antipin *et al.* (1997) distinguished an HFSR type with elevated Zr contents.

Despite the existence of such varieties, all HFSR show similar flat REE distribution patterns. This distribution is characterized by elevated HREE contents and a strong negative Eu anomaly (Burt *et al.*, 1982; Christiansen *et al.*, 1983; Rub and Rub, 1991; Kovalenko *et al.*, 1999). Consequently, there is no direct connection between the accessory mineral association and the manner of REE accumulation in HFSR (Gramaccioli *et al.*, 1999).

There are two interpretations for the nature of the geochemical signature of HFSR: either as a result of accumulation of strongly incompatible elements in residual magmas or as a result of fluid–magma differentiation. This is illustrated by the behavior of Eu in HFSR. The strong Eu depletion in HFSR is considered to be due either to feldspar fractionation during the early stages of rock formation (e.g., Noble *et al.*, 1979) or to preferential Eu removal from melt into fluid by comparison to other REE (Flynn and Burnham, 1978; Zharikov, 1996). Since feldspar comprises no more than 10% of europium in the rocks and no more than 1–2% of other REE (Gromet and Silver, 1983), it is evident that even the complete removal of feldspars cannot provide the observed effect. REE partitioning between HFSR minerals was comprehensively studied by Rub and Rub (1991) and Nash (1993). Their results are in agreement with each other: all the minerals of granitoids show a europium deficit, and the most depleted phases in both cases were plagioclase and potassium feldspar (Fig. 3). These results suggest that feldspar fractionation was not responsible for the formation of the negative Eu anomaly in HFSR. The general depletion of all minerals, both major rock-forming and accessory, in europium (Kovalenko *et al.*, 1979) indicates that the magma was impoverished in this element *before the onset of crystallization.*

The analysis of geochemical data on HFSR reveals a strong correlation between the character of REE distribution and the fluorine content of magmas. This is illustrated in Fig. 4, which shows correlations of Ce/Yb and Eu/Eu* with fluorine in subalkaline silicic lavas and subvolcanic complexes of North America and ongonites (Ivanova *et al.*, 1995; Christiansen *et al.*, 1983; Macdonald *et al.*, 1992; Tsareva *et al.*, 1991).

In contrast to fluorine, chlorine is not correlated with Ce/Yb and Eu/Eu*, which indicates a minor role of chlorine in the process of REE fixation in magmas. Figure 5 shows REE variations in the process of magma differentiation. The LREE/HREE ratio of magmas decreases at the expense of LREE depletion. The analysis of such dependencies shows that bulk REE contents do not increase at HFSR formation, and, therefore, the main reason for the formation of the characteristic REE spectrum is selective LREE removal concurrent with fluorine accumulation in magmas.

The compositions of holocrystalline rocks also show strong correlations between fluorine content and REE distribution patterns. Granitoids lose significant part of their volatiles during subsolidus processes. Because of this, we explored these correlations using the mole fraction of fluor-biotite in mica as an indicator of the fluorine content of magma. This approach is jus-

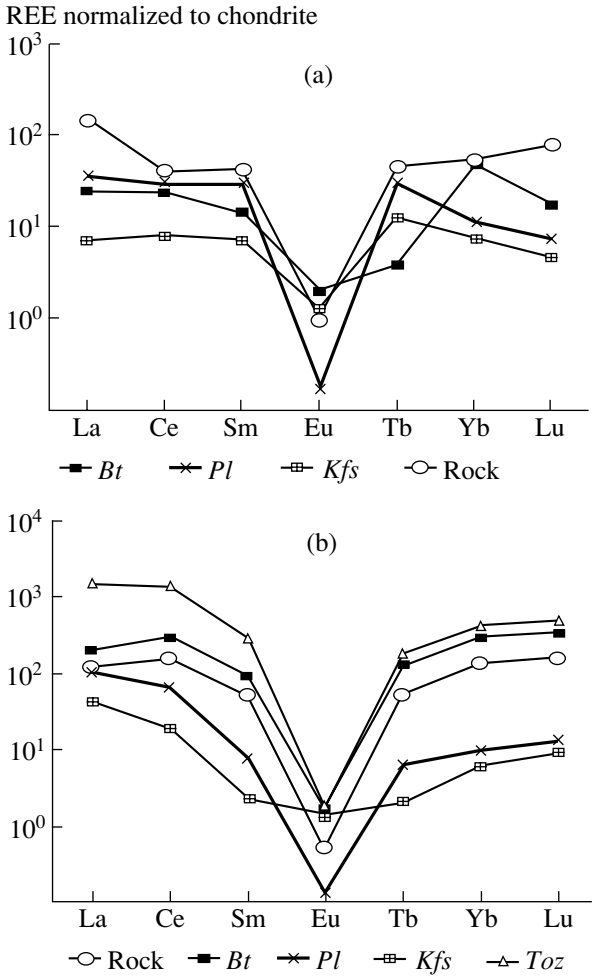

Fig. 3. Chondrite-normalized REE concentrations in HFSR and their minerals: (a) Honeycomb Hills topaz rhyolites (Congton and Nash, 1988; Nash, 1993) and (b) lithium–fluorine granites of Primorie (Rub and Rub, 1991).

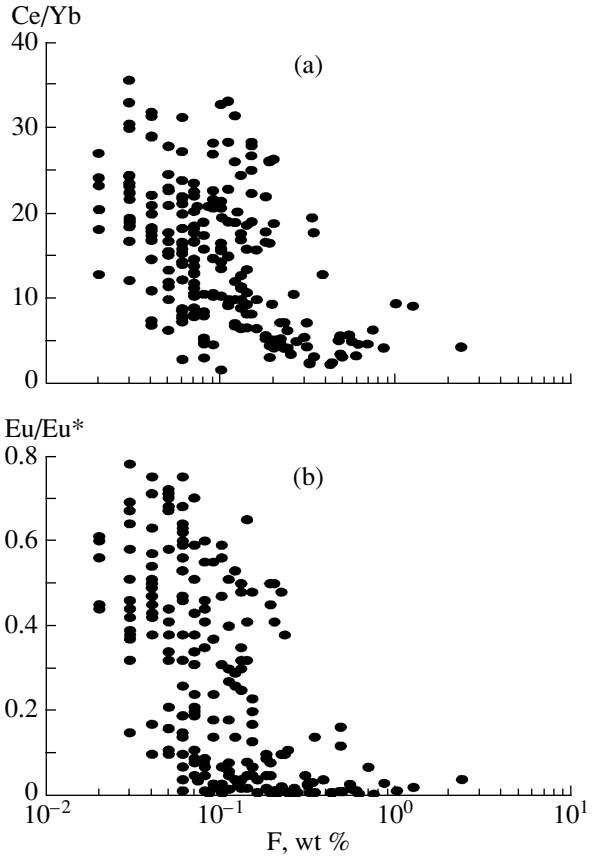

Fig. 4. Correlations (a) Ce/Yb–F and (b) Eu/Eu*–F for the subalkaline silicic lavas and subvolcanic complexes of North America and ongonites (Ivanova *et al.*, 1995; Christiansen *et al.*, 1983; Macdonald *et al.*, 1992; Tsareva *et al.*, 1991; Stix and Gorton, 1990; Nash, 1993).

tified by the correlation of fluorine contents in biotite and magma (Bushlyakov and Kholodnov, 1986; Icenhower and London, 1997). The HFSR of Mongolia and Transbaikalia (Silaev and Vasin, 1989; Budnikov, 1996) and silicic rocks of the USA (Nash, 1990; Tsareva *et al.*, 1991) and central Kazakhstan (Negrei, 1983; Abramov and Borisovskiĭ, 1996) were used as reference objects. Figure 6 illustrates a direct correlation between the fluorine content of biotite (X_{Bt}^{F}) and the REE distribution pattern of the rocks (La/Yb and Eu/Eu*), which is in agreement with the data on glassy rocks.

The concentration of chlorine shows no stable correlation with the same components of fluorine-rich granitoids. According to Kovalenko *et al.* (2000), the concentrations of fluorine and chlorine are not correlated in melt inclusions from silicic rocks. The absence (indifference) of chlorine in the genesis of HFSR was demonstrated by Candela (1986), who established that apatite from unmineralized plutons is often richer in chlorine than apatite from mineralized intrusion. Investigations of melt inclusions from the Pine Grove HFSR (Lowenstern, 1994) showed that the ore-bearing magmas were characterized by F ⩾ Cl. The same fluorine and chlorine relationships are characteristic of the ore-bearing granitoid magmas of central Kazakhstan and Mongolia (Abramov and Borisovskiĭ, 1996; Budnikov, 1996). However, opposite examples can be found: chlorine and fluorine contents are comparable in the magmas of the Chatkal–Kurama porphyry intrusions (Abramov *et al.*, 2001) and Taylor Creek rhyolites (Webster and Duffield, 1994). Thus, HFSR are formed both when chlorine is an important fluid component and when its content is low. This fact allows us to simplify the model composition of the fluid phase of HFSR and ignore processes related to chlorine accumulation.

Thus, the strong correlation of fluorine with the concentrations of major and trace elements in HFSR indicates that the characteristic petrochemical and geochemical features of HFSR are probably related to the processes of fluorine accumulation in magmas. The net effect of fluorine accumulation and redistribution of

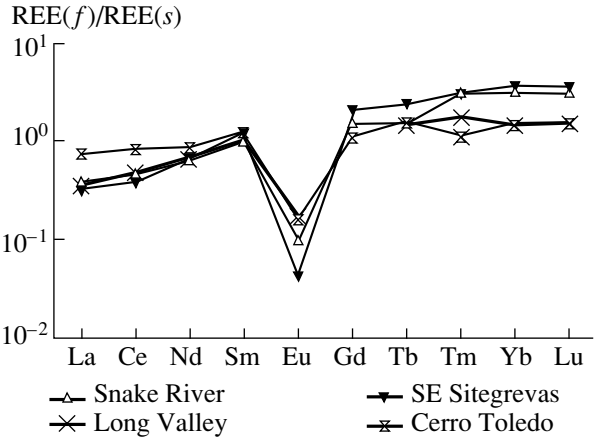

Fig. 5. Ratios of REE concentrations in strongly differentiated HFSR (*f*) and weakly differentiated granitoids (*s*) after Macdonald *et al.* (1992).

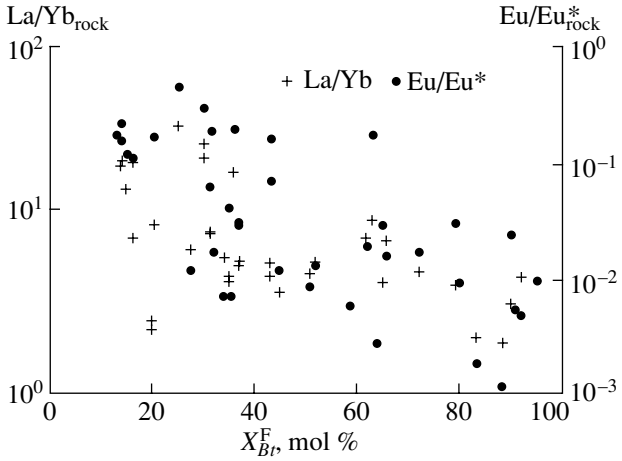

Fig. 6. Relationships of X^F_{Bt} –La/Yb_{rock} and Eu/Eu^*_{rock} for the HFSR of Mongolia and Transbaikalia (Silaev and Vasin, 1989; Budnikov, 1996) and the silicic rocks of the USA (Nash, 1993; Tsareva *et al.*, 1991) and Central Kazakhstan (Negrei, 1983; Abramov and Borisovskiĭ, 1996).

major components during magma generation is the formation of peculiar assemblages. The high alumina content of melts results in the crystallization of topaz and Al-rich micas; and the high Fe/(Fe + Mg + Mn) ratio is reflected in the development of biotite (annite–siderophyllite), magnetite–ilmenite assemblage, and, occasionally, fayalite.

MINERALOGICAL CHARACTERISTICS OF HFSR AND REDOX CONDITIONS OF THEIR FORMATION

The occurrence of iron-rich minerals in HFSR is often used as an argument for the formation of HFSR in a reducing environment. However, the experimental investigation of the equilibrium *Kfs* + *Mag* = *Bt* + H_2 demonstrated that an increase in Fe^{3+} and F contents of biotite significantly expands the stability filed of iron-rich biotite–magnetite assemblage to higher f_{O_2} (Munoz, 1984; Rebbert *et al.*, 1995; Abramov, 2000). Ilmenite is also an index mineral used as an indicator of HFSR reduction (Ishihara, 1977; Ague and Brimhall, 1988; Whalen and Chappel, 1988). The subsolidus cooling of granitoids often results in complete loss of titanium from ilmenite, and the compositions of magmatic ilmenite and magnetite are not preserved. Because of this, *Ilm-Mag* pairs from hypabyssal granitoids never yield reasonable *T*-f_{O_2} estimates. Ague and Brimhall (1988) supposed that the composition of ilmenite is more conservative upon cooling and proposed the following equilibrium for the calculations of *T*-f_{O_2} conditions:

Bt + O_2 = *Kfs* + *Hem* (in ilmenite) + H_2O.

They obtained very low values of oxygen fugacity (QFM – 1 to QFM – 3), which allowed them and Whalen and Chappel (1988) to speculate that oxygen fugacity was controlled during the formation and crystallization of HFSR by graphite that captured by magmas from assimilated wallrocks.

Frost (1991) and Frost and Lindsley (1991) have later shown that the condition of *Ilm* conservation upon subsolidus cooling is not met, and the composition and amount of ilmenite forming during a postmagmatic stage are defined by such factors as the ilmenite/magnetite ratio of the initial magma and *T*-f_{O_2} characteristics of the cooling path. Therefore, only the ilmenite–magnetite oxygen barometer can give correct *T*-f_{O_2} estimates. This conclusion is contrary to that of Ague and Brimhall (1988) on the "graphite" control of f_{O_2}. Biotite equilibria with graphite-saturated COHF fluid were analyzed by Abramov (2000), who showed that biotite isopleths in such a system are fundamentally different from those in equilibrium with pure water fluid. Thus, the mechanical extrapolation of experimental results in OH-systems to graphite-bearing equilibria can lead to erroneous *T*-f_{O_2} estimates. Taking into account this fact, it can be concluded that the hypothesis of reduced HFSR generation via magma contamination with graphite has no sound basis and must be further inspected.

The table shows f_{O_2} estimates for the subvolcanic occurrences of strongly differentiated silicic magmas whose minerals retained the compositions of magmatic minerals and whose magmatic temperature was confirmed by independent methods (geothermometers and melt inclusion studies). The scatter of oxygen fugacity estimates is about 3–5 orders of magnitude, from QFM to HM. Despite this, the HFSR are geochemically similar: they show high Rb contents, low La/Yb, and pronounced europium depletion.

Such a range of oxygen fugacity values in the systems studied prompted us to reconsider the thesis on the reduced character of iron-rich HFSR. The obtained geological and petrologic information suggests that HFSR formation can hardly be described by a single process. The main petrochemical and geochemical features of HFSR are closely related to the process of fluorine accumulation in magmas. Consequently, by finding an approach to the description of the process of fluorine accumulation, we will be able to understand the geochemical signatures of these magmas with respect to other elements.

MECHANISM OF FLUID DIFFERENTIATION

The efficiency of fluid redistribution of fluorine in the apical parts of intrusions is related to the fact that fluorine solubility decreases in ascending fluid and increases in magma with decreasing temperature (Abramov and Rasskazov, 1997). The maximum possible increase in fluorine concentration in the melts of apical zones can be calculated. A simplified model for a degassing silicic intrusion is a cylindrical body, through which magmatic fluid is filtered under variable temperature conditions (Fig. 7). The size of the body is taken in accordance with geophysical estimates as 1 km in vertical extent and 0.4 km in diameter. A chamber of granitic magma occurs in its lower part at a temperature of 800°C. The temperature of the upper part of the apical body is taken to be 650°C (granite solidus). Let us assume that fluid is released from the magma in the lower part of the conduit at a temperature of 800°C. Its fluorine concentration is defined as $C_{fl}^{HF} = C_{0m,800}^{HF}/K_p(800)_{m/fl}^{HF}$ where $C_{0m,800}^{HF}$ is the initial ordinary fluorine concentration in the melt at 800°C, and $K_p(800)_{m/fl}^{HF}$ is the partition coefficient of HF between melt and fluid. If we assume that the amount of fluid is much larger than the amount of melt during filtration in the column (condition of steady-state filtration), the same fluid in equilibrium with magma in the upper part at 650°C will provide the following fluorine concentration in the melt:

$$C(\text{eq})_{m,650}^{HF} = C_{fl}^{HF} \cdot K_p(650)_{m/fl}^{HF},$$

where $C(\text{eq})_{m,650}^{HF}$ is the equilibrium fluorine concentration in the melt reaction product. Consequently, the maximum possible effect of fluorine enrichment in a filtration (metamagmatic) system equals to the ratio of partition coefficients at appropriate temperatures ($K_{pm/fl}^{HF}$) (Kovalenko, 1979):

$$C(\text{eq})_m^{HF}/C_{0m}^{HF} = K_{pm/fl}^{HF}(650)/K_{pm/fl}^{HF}(800)$$
$$= 30\text{–}40/2\text{–}3 = 10\text{–}20 \text{ times}.$$

The real situation must be more complicated. Fluid filtration changes the bulk composition of melt (especially Na and K), which, in turn, affects halogen solubilities in magmas (Kovalenko, 1979; Malinin and Kravchuk, 1995; Chevychelov, 1999). In addition, the key points in the realization of such a model are the presence of an excess fluid phase, fluid permeability of the medium, relationships of heat and mass transfer processes during fluid filtration, and kinetics of fluid–magma exchange.

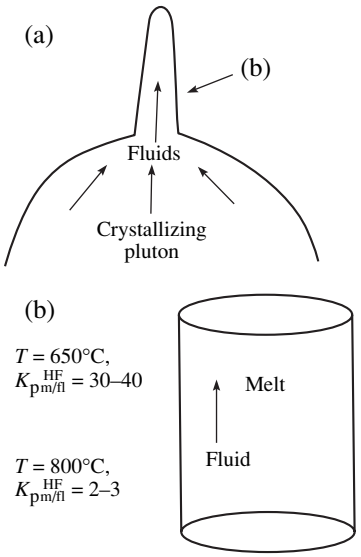

Fig. 7. A schematic description of the model. (a) Crystallization of the main pluton and release of the fluid phase. Fluid moves upward into the apical part of the pluton modeled by (b) the cylindrical body through which magmatic fluid is filtered. Temperature is 650°C in the upper part of the body and 800°C in the lower part; also shown are the values of fluorine partition coefficients between melt and fluid for these temperatures.

Magma crystallization under isobaric conditions (retrograde boiling) results in the appearance of a free fluid phase (Westrich *et al.*, 1988). This produces excess pressure, which was estimated by Tait *et al.* (1989) as up to 100–150 bar even at moderate degrees of magma crystallization (20–30%). Stix and Layne (1996) established that the Cerro Toledo silicic system (New Mexico) occurred before the catastrophic eruption in a state of passive degassing compensating considerable excess pressure (>750 bar). Although scenarios of the behavior of degassing silicic systems have been repeatedly addressed (Taylor *et al.*, 1983; Westrich *et al.*, 1988; Candela, 1986a, 1992; Lowenstern, 1994; Shinohara and Kazahaya, 1995), the form of fluid release from the melt during passive degassing is not exactly known. It is supposed that fluid is removed as either vesicles or films. The physical aspects of these mechanisms have been discussed by Candela (1991, 1992), Shinohara and Kazahaya (1995), Gibert *et al.* (1999), and Balashov *et al.* (2000). Shinohara and Kazahaya (1995) and Cardoso and Woods (1999) demonstrated that the bubble degassing mechanism is predominant in the magmas that show

low degrees of crystallization and are capable of convection. When the medium becomes heterophase (crystalline mush near the contact), the effective ascent of a bubble is halted. Other permeability mechanisms related to the presence of phase boundaries in the crystal mush develop under such conditions. The morphology of phase boundaries is controlled by the wetting angle (Θ). There is no data on the geometry of the melt–fluid interface. Estimates of Θ for fluid–mineral interfaces show the contrasting behavior of water–salt and water–carbon dioxide fluids (Brenan, 1991; Gibert *et al.*, 1998). H_2O-CO_2 fluid ($\Theta > 60°$) forms vesicles on crystal surfaces, whereas H_2O–NaCl fluid ($\Theta < 60°$) fills the system of connecting channels on the interface. Gibert *et al.* (1999) demonstrated for the granulite–heterophase fluid (H_2O-CO_2 + H_2O-NaCl) system that only H_2O–NaCl fluid films are capable of filtering, whereas low-density water–carbon dioxide fluid occurs as unmovable bubbles. Thus, in the heterogeneous H_2O-CO_2–NaCl fluid system, the water–chloride phase is mobile and can be removed from the rock or crystal mush, whereas water–carbon dioxide vesicles cannot migrate. Since HFSR formation occurs within a rather wide temperature range from 800–900°C (very low degree of crystallization) to 650–600°C (latest intervals of rock crystallization), it is reasonable to suggest that fluid is efficiently removed from melt by a combination of degassing mechanisms: vesicle ascent through magmas in the lower part of the chamber and filtration of fluid films in the heterophase aggregate of the apical part of the magmatic cupola.

Permeability of the Medium

Despite the excess pressure in the chamber, the high permeability of magmatic melts prevents magma discharge by extrusion or explosion, and the fluid is filtered upward from the main magma chamber in accordance with the pressure gradient through apical magmatic bodies (conduits). The complex problem of fluid transport through magmas is not yet fully solved. Three permeation mechanisms have been supposed: (1) through a system of immovable gas bubbles; (2) through pores in silicate foam; and (3) through crystal aggregates.

Candela (1991, 1992), Candela and Blevin (1995), and Blower (2001) argued that magma permeability in the apical parts of silicic plutons is related to the formation of the heterophase system silicic melt + low-density gas phase + water–salt fluid. The fluid-transporting element of this model is represented by a system of interconnected gas bubbles, and the movable medium is water–salt fluid. The experiments of Simakin and Épel'baum (1998) on the vesiculation of silicic magmas demonstrated that, even during initial stages of magma boiling, vesicles usually connect to form chains and bands in melt. Modeling of the dynamics of magma vesiculation (Proussevitch and Sahagian, 1996) showed that at high pressures a system of interconnected vesicles is not formed even at high degrees of magma oversaturation with respect to fluid, and the occurrence of such a mechanism of fluid filtration through magma is restricted to small depths.

Stix and Layne (1996) calculated the dynamic parameters of degassing of the Cerro Toledo silicic system using the model of silicate foam. Foamed structures were experimentally reproduced by Letnikov *et al.* (1990) by the rapid decompression of silicic magmas. However, it is not clear if this permeability mechanism can operate for a long time and provide steady-state fluid filtration.

The experimental study of the mechanical properties of partially molten basalts (Philpotts and Carroll, 1996) demonstrated that the permeability of a melt containing ~67% of crystals approaches that of sandstone and is related to the formation of crystal bands and chains.

The estimation of permeability for mechanisms (1)–(3) shows rather high values. The model of Candela yields a permeability of 10^{-7}–10^{-9} cm^2 (Abramov and Rasskazov, 1997). Similar permeability values were obtained by Blower (2001) for the same model. Stix and Layne (1996) estimated the permeability of foamed rhyolites as 10^{-6} cm^2. The measured permeabilities of natural pumices are within 10^{-12}–10^{-8} cm^2 (Eichelberger *et al.*, 1986). Calculations from the experimental data on the partial melting of basic rocks yield permeability values within the range 10^{-5}–10^{-6} cm^2 (Philpotts and Carroll, 1996). The values of permeability obtained for the three mechanisms are much higher than the permeability of solid igneous rocks (10^{-8}–10^{-16} cm^2, Shmonov *et al.*, 1994; Oelkers, 1996). Future work should answer the question of the most important mechanism of melt permeability. It is possible that a combination of these extreme models is realized in nature.

Dynamic Constraints

The ascending fluid must be oversaturated with respect to fluorine and other components relative to magma. Efficient fluid transport requires that

(1) $j_{conv} > j_{diff}$, where j_{conv} is the matter fluxes related to moving fluid, and j_{diff} is the diffusion flux from fluid to magma (mol cm^3/s);

(2) $t_h > t_{ex}$, where t_h is the time of achievement of thermal equilibrium between magma and fluid (i.e., the time of convective heating), and t_{ex} is the time of achievement of chemical equilibrium between magma and fluid.

The former constraint results in the disturbance of local equilibrium, which is necessary to create the flux of matter (fluorine and other components) from fluid to magma. The latter condition implies that changes in the concentrations of dissolved components (HF and others) in the ascending fluid must occur slower than the process of thermal equilibration. Since fluorine solubil-

ity in fluid decreases with decreasing temperature, condition (2) results in that the fluid is always oversaturated in this component under given temperature.

Kinetics of Fluid–Melt Interaction

The estimated times of chemical equilibration for the two extreme models of melt degassing, filtration of fluid films through interconnecting channels along the fluid/crystal/melt interfaces (Abramov and Rasskazov, 1997) and ascent of vesicles through magma (Épel'baum, 1978), differ by several orders of magnitude (2–50 y and 10–1000 h, respectively). In the former case, diffusion in a stagnant layer at the fluid/magma boundary was considered as the limiting stage of exchange; and in the latter case, it was assumed that internal circulation occurs in a moving fluid vesicle, which accelerates mass exchange and prevents boundary layer formation. The very high rates of mass exchange in a vesicle moving through magma suggest that degassing via the vesicle mechanism in the lower part of the magma chamber occurs under equilibrium conditions (Épel'baum, 1978; Shinohara, Kazahaya, 1995).

The rate of chemical exchange between fluid films and melt in the upper cupola part of the chamber must be limited by the slowest stage of exchange, diffusion in the stagnant boundary layer of fluid. The transport of matter through the walls of fluid channels into magma can be regarded, therefore, as a diffusion flux. Since the matter is not accumulated in the boundary layer and $D^{HF}_{fluid} > D^{HF}_{melt}$ (Chekhmir *et al.*, 1991), the intensity of diffusion flux must be determined from the values of diffusion rates in the melt. Since the geometry of the permeable medium is poorly constrained, j_{diff} is estimated as diffusion fluxes through a plane, a cylinder, and a sphere; the real matter flux is a combination of these simple cases. The respective fluxes (mol cm^3/s) are (Chizmadzhev *et al.*, 1971)

$$j = DKA\frac{\Delta C}{\delta l},$$

$$j = 2\pi DK\frac{\Delta C}{\ln(r/\delta l)},$$

and

$$j = 4\pi DK\frac{\Delta C r\delta l}{(r-\delta l)},$$

where D is the diffusion coefficient of HF in the melt, K–$K^{HF}_{pm/fl}$, ΔC is the gradient of HF concentration (molar), A is the surface area, r is the cylinder or sphere radius (0.01 cm), and δl is the diffusion boundary layer (Kokotov and Pasechnik, 1970). The quantity δl is estimated as

$$\delta l/\delta l_0 = \left(\frac{D^{H_2O}}{\nu}\right)^{1/3},$$

where $\delta l_0 = 5\ (\nu X/u)^{0.5}$ (Kutepov *et al.*, 1996), X is the length of the channel, δl_0 is the hydrodynamic boundary layer, D^{H_2O} is the diffusion coefficient of water in the fluid, and ν is the kinematic viscosity of the fluid.

The convective flux is estimated as $j_{conv} = qC_iA_f$, where q is the specific liquid discharge (cm/s), C_i is the concentration of the component in the flow; and A_f is the cross-section area of the conduit.

The following initial values were accepted to calculate the vertical fluid velocity: an excess pressure of 100 bar and a permeability of 10^{-7}–10^{-8} cm^2. Since the degassing pluton is a "failed" volcano, it is reasonable to estimate the vertical extent of the magmatic body, where the mechanism of retrograde boiling operates effectively, as the critical size of a magma column that can be removed under the influence of fluid defragmentation during ignimbrite eruption. The estimates by Wolff *et al.* (1990) for the thickness of such a layer are within H = 100–500 m for silicic systems.

Under such parameters, the Darcy filtration equation yields the specific liquid discharge (cm/s) $q = \frac{k\Delta P}{\mu H}$, where k is the permeability coefficient (cm^2), μ is the dynamic viscosity (Pa s), and H is the vertical interval (cm) of the influence of pressure gradient ΔP. Since the fraction of connected pores is usually lower than 100%, the rate of filtration in a porous medium is higher than the specific discharge by the value ϕ (specific fraction of connected pores): $u = q/\phi$. The parameter ϕ is difficult to determine and varies from 0.01 to 0.5 (Lichtner, 1996). It can be taken as 0.1 for approximate calculations. The calculated vertical filtration velocity varies depending on the thickness of the magmatic body from 2 cm/s to the lowest value of 0.01 cm/s.

These estimates suggest (Fig. 8) that, when u is within 0.1–2.0 cm/s, the condition $j_{conv} > j_{diff}$ holds at any geometry of the medium. If the rate of filtration is $u \le 0.1$ cm/s, the geometry of the permeable medium can be the critical factor. If flat channels are predominant, the diffusion mass transfer is considerable and is higher than the convective mass transfer by fluid at filtration rates $u \le 0.1$ cm/s. The predominance of cylindrical and spherical elements at the fluid/magma interface decreases the critical velocity. Taking into account that flat channels are essentially lacking in models (1)–(3) of melt permeability, and the morphology of permeable elements approaches cylinders (channels) and spheres (bubbles), the values of $j(D)$ must be calculated as a combination of diffusion fluxes from a sphere and a cylinder and are lower than the convective mass transfer.

Relationships of Heat and Mass Transfer Processes

The ascending fluid is a heat carrier, and, consequently, filtration causes heating of the permeable body. If the rate of heat transfer (v_T) is equal to or higher than

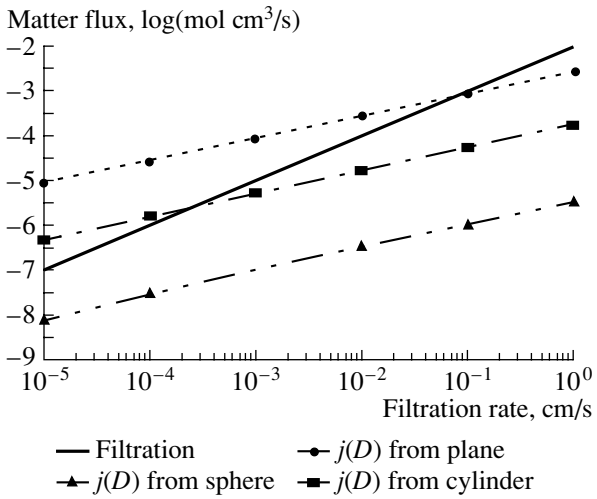

Fig. 8. Relationships of j_{conv} and j_{diff} values for various rates of fluid filtration. See text for further explanation.

the rate of mass transfer (v_ε), fluorine will not be redistributed from fluid to magma.

As the most reliable estimate for the relationship of these parameters, we can calculate the time of thermal equilibration (t_h) between the magma of the root and apical zones (e.g., the time of convective heating) and the time of chemical equilibration (t_{ex}) between magma and fluid under lowest temperatures. If $t_h > t_{ex}$, the relation $v_T > v_\varepsilon$ holds in all parts of the filtration column and the mechanism of fluid fluorine redistribution is efficient.

Previous estimates by the equation of the convective cooling of intrusions (Criss and Taylor, 1986) for this model (t_h = 500–5000 y; Abramov and Rasskazov, 1997) are consistent with estimates obtained by other methods. The 2D modeling of the convective heating of rocks above intrusion roofs (program Heat, version 3.8; Woheltz and Heiken, 1991) yielded t_h estimates of ≈10000 y. Another independent method for t_h estimation is the determination of the heating time of the blocks of roof rock that were moved to the surface during the eruption of Mount Mazama Volcano (Bacon, 1992). The duration of heating up to melting temperature was estimated from the size of glass fringes around *Pl*, *Zrn*, and *Mag* crystals, which were formed owing to rock heating. These t_h estimates range from 100 to 10000 y. However, the minimum value can be underestimated, because, at a certain time moment, the roof rocks were disintegrated into blocks 1–4 m across, which accelerated heating processes. The maximum values are therefore preferable for the estimation of the time of melting of large rock blocks.

Thus, t_h values obtained by various methods are mutually consistent and range within 5000–10000 y. Consequently, the model condition $t_h > t_{ex}$ holds. This allows us to use this model for the description of the behavior of some components in the process of fluid–magma interaction.

MODELING OF FLUID DIFFERENTIATION: THE BEHAVIOR OF VOLATILE COMPONENTS, REE, AND IRON

Oxygen

The influence of degassing on the degree of melt oxidation was evaluated by Candela (1986b), who quantified the effect of hydrogen removal as the most volatile component of magmas. Taking into account coupled reactions in magma and fluid, it was shown that prolonged degassing would result in the appearance of oxidized (up to the HM buffer) and iron-poor magmas. Thus, this model cannot explain the formation of iron-rich magmas with varying oxidation states. In addition, Chekhmir *et al.* (1991) showed that the influence of preferential hydrogen removal from magma on oxygen fugacity must be insignificant. Since the transport of H_2 is accompanied by redox reactions, its real transport velocity in melt is equal to that of the front of the redox reaction $H_2 + 0.5O_2 = 0.5H_2O$ and is similar to the rate of molecular water migration in melt.

Consider fluid filtration through a magmatic column under conditions of a temperature gradient from 800°C in the lower part of the chamber to 600°C at the upper contact (completely crystallized rock).

The thermal equilibration of fluid filtering upward through cooler magma occurs almost instantaneously (Candela, 1991). Therefore, fugacities of components must change in cooling fluid, because the bulk fluid composition is conserved ($j_{conv} > j_{diff}$) and gas reactions in fluid are very fast (compared to the rate of fluid/magma exchange).

In order to determine variations in oxygen fugacity in ascending fluid, it is necessary to calculate how the molecular composition of fluid changes in response to temperature and (or) pressure variations at constant atom proportions. Fluorine compounds of silicon and aluminum occur in fluid at high HF concentrations (Haselton *et al.*, 1988; Aksyuk and Zhukovskaya, 1998), but we can simplify fluid composition for the problem formulation, because of the negligible influence of these compounds on oxygen balance. The composition of fluid is defined by X_{H_2O}, X_{H_2}, X_{SO_2}, X_{H_2S}, X_{CO}, X_{CH_4}, X_{HF}, X_{S_2}, and X_{F_2}. Let us assume that $X_{S_2} \approx 0$, $X_{F_2} \approx 0$, and $X_{O_2} \approx 0$. Then, the atomic fractions of S, F, C, O, and H are

$$X_S = X_{SO_2} + X_{H_2S}, \quad (1)$$

$$X_F = X_{HF}, \quad (2)$$

$$X_C = X_{CO} + X_{CH_4} + X_{CO_2}, \quad (3)$$

$$X_H = 2X_{H_2O} + 2X_{H_2} + 4X_{CH_4} + X_{HF} + 2X_{H_2S}, \quad (4)$$

$$X_O = X_{H_2O} + 2X_{SO_2} + X_{CO} + 2X_{CO_2}. \quad (5)$$

Note that

$$1 - X_S = X_{H_2O} + X_{H_2} + X_C + X_F$$

and

$$X_{H_2O} + X_{H_2} = 1 - X_S - X_C - X_F. \quad (6)$$

Proceeding from the reactions

$$H_2 + 0.5O_2 = H_2O, \text{ (I)}$$

$$H_2 + 0.5S_2 = H_2S, \text{ (II)}$$

and

$$O_2 + 0.5S_2 = SO_2, \text{ (III)}$$

we obtain

$$X_{H_2O} = f_{H_2O}/P_{total}\gamma_{H_2O} = (K_{pI} f_{H_2} f_{O_2}^{0.5})/(P_{total}\gamma_{H_2O}) = K_{H_2O} f_{H_2} f_{O_2}^{0.5}, \quad (7)$$

$$X_{H_2S} = K_{H_2S} f_{H_2} f_{S_2}^{0.5}, \quad (8)$$

$$X_{SO_2} = K_{SO_2} f_{O_2} f_{S_2}^{0.5}, \quad (9)$$

$$X_{H_2} = f_{H_2}/K_{H_2}, \quad (10)$$

where $K_j = K_{pn}/P_{total}\,\gamma_j$ (j is H_2O, H_2S, or SO_2) and $K_{H_2} = 1/P_{total}\gamma_{H_2}$.

Then,

$$K_{H_2O} f_{H_2} f_{O_2}^{0.5} + f_{H_2}/K_{H_2} = 1 - X_S - X_C - X_F, \quad (11)$$

and

$$f_{H_2} = (1 - X_S - X_C - X_F)/((K_{H_2O} f_{O_2}^{0.5}) + K_{H_2}). \quad (12)$$

Considering the reactions

$$CO_2 = CO + 0.5O_2, \text{ (IV)}$$

and

$$CO + 2H_2 = CH_4 + 0.5O_2, \text{ (V)}$$

we obtain

$$X_{CO} = f_{CO}/P_{total}\gamma_{CO} = f_{CO}/K_{CO}, \quad (13)$$

$$X_{CO_2} = f_{CO} f_{O_2}^{0.5}/K_{pIV} P_{total}\gamma_{CO_2} = f_{CO} f_{O_2}^{0.5}/K_{CO_2}, \quad (14)$$

$$X_{CH_4} = f_{CO} f_{H_2}^2 K_{pV}/f_{O_2}^{0.5} P_{total}\gamma_{CH_4} = f_{CO} f_{H_2}^2/(K_{CH_4} f_{O_2}^{0.5}), \quad (15)$$

$$f_{CO} = X_C/(K_{CO} + f_{O_2}^{0.5}/K_{CO_2}) + f_{H_2}^2/(K_{CH_4} f_{O_2}^{0.5}). \quad (16)$$

Similarly, we can write for sulfur compounds:

$$X_S = f_{S_2}^2 (f_{O_2} K_{SO_2} + f_{H_2} K_{H_2S}), \quad (17)$$

$$f_{S_2}^{0.5} = X_S/(f_{O_2} K_{SO_2} + f_{H_2} K_{H_2S}). \quad (18)$$

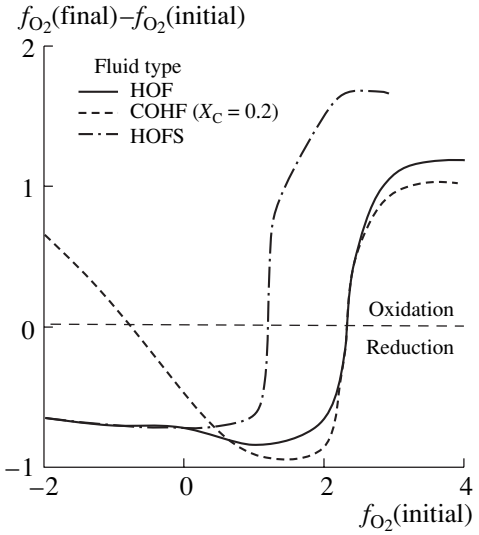

Fig. 9. The effect of the filtration of fluids of various compositions on the oxygen fugacity of host magmas. In all initial fluid compositions, $\log f_{H_2O}/\log f_{HF} = 2.8$; the initial compositions of HOFS fluids at $f_{O_2} <$ QFM – 1 were calculated in equilibrium with pyrrhotite. The initial oxygen fugacity in fluid at 827°C is show along the *x* axis relative to QFM (i.e., $\log f_{O_2} - \log$QFM); and variations in oxygen fugacity during fluid cooling to 627°C is shown in logarithmic units along the *y* axis.

Then, Eq. (5) can be recast as

$$X_O = f_{H_2} f_{O_2}^{0.5} K_{H_2O} + 2 f_{S_2}^{0.5} f_{O_2} K_{SO_2} + f_{CO}/K_{CO} + 2 f_{CO} f_{O_2}^{0.5}/K_{CO_2}. \quad (19)$$

After substituting f_{H_2} from Eq. 12 into Eqs. 16 and 18, and f_{CO} and f_{S_2} from Eqs. 16 and 18 into Eq. 19, f_{O_2} can be found as a function of the atomic composition of fluid under given pressure and temperature values.

The calculation of variations in oxygen fugacity during cooling of COHF fluid is illustrated in Fig. 9. It appears that, if the initial oxygen fugacity is higher than QFM +1...+2, fluid filtration under temperature-gradient conditions leads to an increase in f_{O_2}, whereas the opposite effect is predicted for the filtration of fluid whose initial oxygen fugacity is lower than QFM +1...+2. It is evident that prolonged fluid filtration through magma must produce corresponding changes in oxygen fugacity in the melt. The absolute value of f_{O_2} increases with decreasing temperature and addition of sulfur-bearing gases into the system, but the boundary QFM +1...+2 between the oxidizing and reducing trends persisted in all the compositions calculated. Thus, fluid filtration through the magmas of apical zones must produce either oxidized or reduced magmas.

Fluorine and Water

Modeling the process of fluorine redistribution between filtered fluid and magma requires the knowledge of changes in the partition coefficient $K_{pm/fl}^{F}$ during fluid ascent through magma. According to Kovalenko (1979), this parameter depends primarily on temperature and fluorine content in the magma, and decreases with increasing temperature and bulk concentration. The experiments by Webster (1990) confirmed this dependency and expanded the experimentally studied field to higher F concentration (up to 10000 ppm in melt) and temperature (up to 900°C). For our purposes we interpolated the data of Kovalenko (1979) and Webster (1990). The whole experimental dataset was preliminarily divided into temperature intervals of 550–600, 650–700, 750–800, and 900–1000°C. The interval estimates were combined then in the single parametric equation

$$X_{melt}^{F} = b(X_{fluid}^{F})^{a}, \quad (20)$$

where

$$a = 25.22 - 0.134T + 2.67 \times 10^{-4}T^2 - 2.3 \times 10^{-7}T^3 + 7.26 \times 10^{-11}T^4, \quad (21)$$

and

$$b = 2988.19 - 7.01T + 4.30 \times 10^{-3}T^2$$

X_{melt}^{F}, X_{fluid}^{F} are in ppm and T is in °C.

Thus, if fluid with an initial HF concentration of $X_{fluid,0}^{F}$ is filtered through magma, the quasi-equilibrium fluorine concentration in the melt related to fluorine migration from the fluid will be controlled by X_{fluid}^{F} and temperature of the enclosing magma.

A quasi-equilibrium approximation for water redistribution between fluid and magma can be derived in a similar manner. To this end, we used the expression of Moore *et al.* (1995) for the molar fraction of water as a function of water fugacity in fluid:

$$2\ln X_{H_2O}^{melt} = \frac{a}{T} + \sum_i b_i X_i\left(\frac{P}{T}\right) + c\ln f_{H_2O}^{fluid} + d, \quad (22)$$

where P is the pressure (bar), T is the temperature (K); and a, b, c, and d are coefficients.

As was shown above, atom proportions remain unchanged in a rapidly filtered fluid but the concentrations of molecular species are variable. For example, under given bulk fluorine and water contents, the proportions of F_2 and HF, and H_2O, H_2, and O_2 will vary. Under given temperature gradient and known initial atomic composition, the fugacities of O_2, HF, and H_2O in filtered fluid can be determined by the solution of the system of equations 1–6. These values and temperature gradient allow us to calculate changes in the concentrations of fluorine and water in the melt using Eqs. 20 and 22. Figure 10a shows an example of the calculation of the metamagmatic influence of fluid on magma under a temperature decrease in the filtration column from 827 to 550°C (in the deep source, oxygen fugacity in magma corresponded to QFM + 0.5 and $\log f_{H_2O}/f_{HF} = 2.8$). For comparison, Figure 10b shows changes in magma parameters in sequential portions of the Cerro Toledo ignimbrites. The character of changes in f_{O_2} and fluorine content is consistent with the tendencies calculated for the development of metamagmatic processes: oxygen fugacity declines in sequential magma portions, fluorine content in magma increases, and water content remains approximately constant. Although the results are qualitatively consistent, there is no complete coincidence. To the author's knowledge, there are no publications on the estimation of magma state at a certain time moment in different sections of the magma column, and only such estimates can be directly compared with our model results.

REE

The available thermodynamic data for dissolved REE fluoride and chloride species (Haas *et al.*, 1995) allow us to model the processes of element dissolution in fluoride–chloride solutions, i.e., to simulate situations similar to the development of HFSR. Data on thoroughly studied magmatic systems can be used to assess fluid and melt compositional parameters for modeling. In particular, the observed La/Yb and Eu/Eu* correlations with the fluorine content of biotite (Fig. 6) allowed us to estimate the HF fugacity under which the common REE distribution patterns of HFSR were formed as $\log f_{HF}$ from –0.5 to +0.5.

The process of REE redistribution between fluid and silicic melt can be specified by the schematic reactions

$$12HF(fl) + 2Ln_2O_3(m) = 6H_2O(m) + 4LnF_3(fl), \quad (VI)$$

and

$$2YbF_3(fl) + La_2O_3(m) = Yb_2O_3(m) + 2LaF_3(fl), \quad (VII)$$

where the lanthanide (Ln) oxides are related to species dissolved in the melt and the fluorides are fluid compounds. Reaction (VI) reflects the process of REE redistribution between fluid and melt, and reaction (24) describes the process of preferential accumulation of particular REE (for instance, HREE) in magma in comparison to another REE group. Reactions (VI) and (VII) must be written for both divalent and trivalent forms of europium under variable oxygen fugacity.

The description of heterophase equilibrium requires the knowledge of REE solubility both in solution and in magma. Experiments on REE partitioning between immiscible melts (Ellison and Hess, 1989) demonstrated that activity coefficients of heavy and light REE in silicic melts are of the same order of magnitude.

Consequently, if

$$a^{melt}_{Ln_2O_3} = X^{melt}_{Ln_2O_3}\gamma_{Ln_2O_3} \text{ then}$$

$$a^{melt}_{REE1}/a^{melt}_{REE2} = X^{melt}_{REE1}/X^{melt}_{REE2}.$$

Under such assumptions, the following equality must hold:

$$\frac{D^{fl/melt}_{REE1}}{D^{fl/melt}_{REE2}} = \frac{C^{fl}_{REE1}}{C^{melt}_{REE1}}\frac{C^{melt}_{REE2}}{C^{fl}_{REE2}},$$

where $C^{melt}_{REE1} = C^{melt}_{REE2}$. Proceeding from these considerations, it was accepted that the initial concentrations of all REE were 0.1 mol Ln_2O_3, which corresponds to ≈0.14 wt % of each lanthanide oxide in silicic melt. Calculations were carried out using the Balance program (Akinfiev, 1986), which relies on the SUPCRT 92 thermodynamic database (Johnson *et al.*, 1992). The fugacity of HF varied from 0.5 to 4.0 bar ($\log f_{HF}$ between –0.5 and 0.5), and the chlorine concentration corresponded to 0.1 m NaCl. The distribution of REE between water–chloride–fluoride fluid and melt was modeled.

According to the calculations, all REE (except for Eu) are weakly soluble in fluid at 800°C, and trace concentrations of hydroxyl REE compounds are predominant (Fig. 11). Substantial REE concentrations in the fluid phase (up to 0.015 mol/kg) were noted at temperatures below 650°C, and this REE enrichment was due to the formation of fluoride complexes. The values of REE concentrations in the solution are comparable to those determined in magmatic fluids equilibrated with topaz granitoids (Rankin *et al.*, 1992). According to our results, the fluoride fluid is relatively enriched in light REE ($La^{fl}/Yb^{fl} = 83$ and $Ce^{fl}/Lu^{fl} = 9$). These calculations are qualitatively consistent with the experimentally measured relationship $D^{fl/melt}_{LREE}/D^{fl/melt}_{HREE} \approx 1.5–6$ (Flynn and Burnham, 1978; Candela and Piccoli, 1995).

The character of europium solubility is different from that of other REE. Within a wide range of oxygen fugacity (from QFM – 2 to QFM + 2), EuO was oxidized in the final products to Eu_2O_3, and the concentration of europium in the solution was several orders of magnitude higher than those of other REE. A series of computations with variable $\log f_{O_2}$ and $\log f_{HF}$ demonstrated the predominance of soluble divalent europium species within the whole range of oxygen fugacity. This is in agreement with the calculations by Sverjenski (1984), who showed that within a wide range of temperature and oxygen fugacity, Eu in solutions occurs in a divalent state. In response to an increase in oxygen activity, the fraction of divalent europium in the solution declines, which, in turn, causes a general decrease in the europium content of solution. At low $\log f_{HF}$ values (between –2 and –4), chloride europium species are predominant in solutions

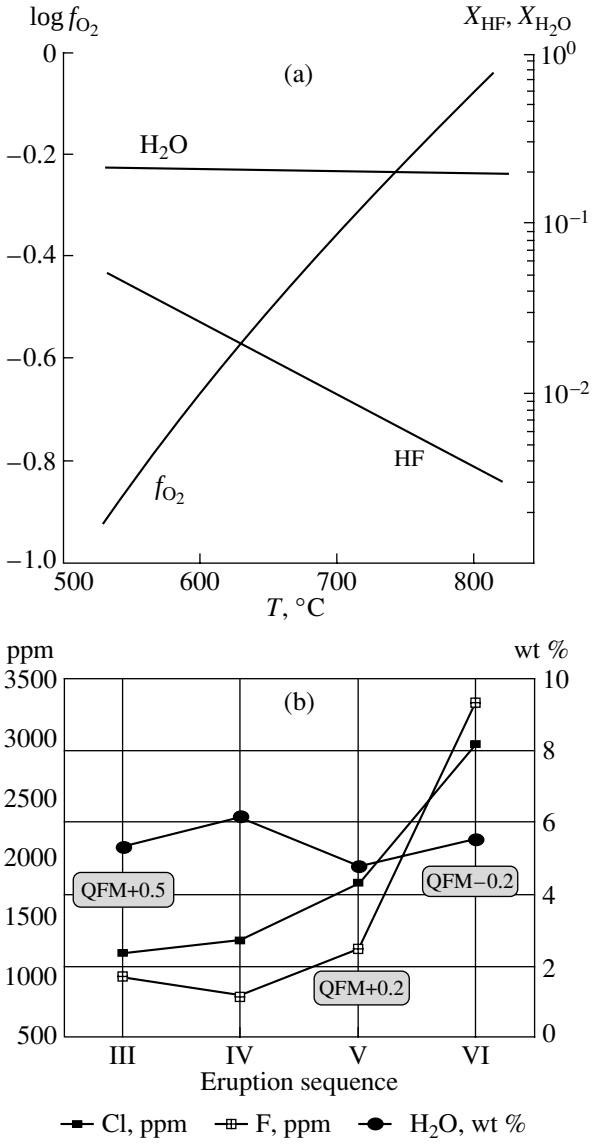

Fig. 10. (a) Effect of changes in f_{O_2}, $X^{H_2O}_{melt}$, X^{HF}_{melt} in the course of fluid filtration through magma. Initial conditions: 827°C, f_{O_2} = QFM + 0.5, and $\log f_{H_2O}/\log f_{HF} = 2.8$. (b) Variations in fluorine and chlorine (ppm) and water (wt %) contents in magmas representing the sequential portions of the Cerro Toledo ignimbrites (Stix and Layne, 1996). The labels show oxygen fugacity values for the given ignimbrite composition.

and their concentrations decrease slightly with increasing oxygen fugacity (Fig. 12). At high HF fugacities ($\log f_{HF} \geq –0.5$), europium concentrations increase owing to the formation of soluble fluoride compounds (mainly, EuF_2aq and EuF_3^-). Fluoride compounds comprise 60–70% of all dissolved europium. Europium solubility in a fluoride environment is much more sensitive to oxygen fugacity variations. The solubility of

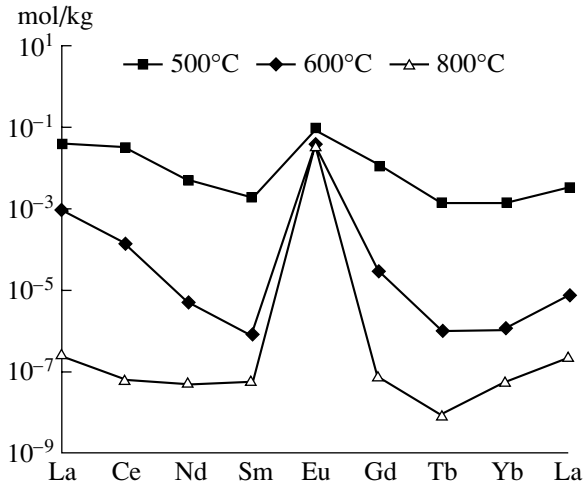

Fig. 11. Calculated REE concentrations in fluid (mol/kg) for temperatures of 500, 600, and 800°C at 2 kbar, f_{O_2} = QFM, $\log f_{HF}$ = 0.5, and 0.1 m NaCl in equilibrium with a magma containing 0.14 wt % of each element oxide.

europium in a reducing environment (QFM – 2) is three times higher than that under QFM oxygen fugacity conditions. Within the whole range of oxygen fugacity (from QFM – 2 to QFM + 2), europium is much more soluble than other REE. For instance, at 600°C, f_{O_2} values corresponding to QFM, and $\log f_{HF}$ = 0.5, europium contents are higher by 3–4 orders of magnitude than those of Sm and Gd (Fig. 11). Thus, our calculations suggest that filtration of fluoride fluid through magma can considerably change REE distribution in the melt. Silicic magmas can be severely depleted in europium as a result of its selective extraction by fluoride fluid, which is later removed from the melt (open degassing model). Such a fractionation may occur within a wide range of oxygen fugacity, which is consistent with the empirical observation that a negative europium anomaly occurs in magmas with widely varying f_{O_2} (Noble *et al.*, 1979). Another important inference from the results of modeling is related to the elucidation of the conditions of light and heavy REE fractionation in silicic magmas. The calculations show that the concentrations of LREE and HREE in fluid are very low at high temperatures (700–800°C). The solubility of light REE in fluid begins to rise at the solidus temperatures of granitic systems, 650°C and lower. Thus, the flat REE distribution patterns related to LREE removal from magmas must be generated within this temperature range. At first glance, this conclusion is contrary to the fact that such REE distribution patterns are observed both in high-temperature subvolcanic HFSR and in relatively low-temperature lithium–fluorine granitoids. In fact, the universality of geochemical features is indirect evidence that all HFSR with flat REE spectra experienced a low-temperature fluid reworking of the apical parts of plutons at some stage of their development (Abdel-Rahman and Martin, 1990).

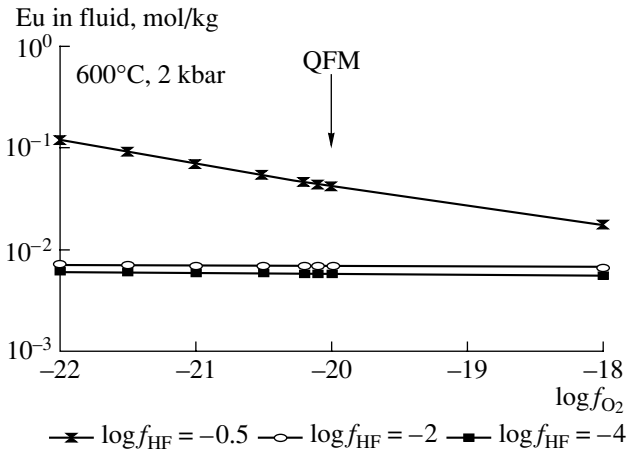

Fig. 12. Calculated europium concentrations in fluid (mol/kg) at various values of $\log f_{HF}$ and $\log f_{O_2}$ for a temperature of 600°C, 2 kbar, and 0.1 m NaCl in equilibrium with a magma containing 0.14 wt % Eu_2O_3.

Iron and Magnesium

The partitioning of major components between magmatic fluid and melt is rather thoroughly studied. However, the comparative behavior of Fe and Mg in high-temperature fluoride solution was never specially

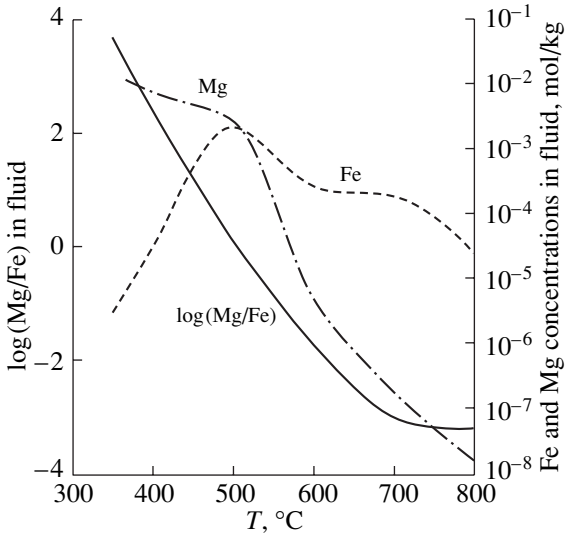

Fig. 13. Calculated temperature dependencies of Fe/Mg ratio in fluid and absolute concentrations of soluble Fe and Mg compounds (mol/kg) at f_{O_2} = QFM, $\log f_{HF}$ = 0.5, and 0.1 m NaCl in equilibrium with *Kfs*, *Bt* (X_{An} = 0.8), *Fa*, *Mag*, and *Qtz*.

investigated. Chevychelov and Épel'baum (1985) reported a slight decrease in iron solubility in 1 m NaCl aqueous solutions (T = 550–600°C), when HF was added to the system. In the context of the model developed here, it is necessary to determine changes in the concentrations of these elements in magmatic fluid at decreasing temperature within a wide range of oxygen activity.

The procedure of calculation is similar to that described for REE. The partitioning of iron and magnesium between fluid and melt is controlled by a series of exchange reactions:

$$Phl + 3FeF^+ = Ann + 3MgF^+,$$

$$Phl + 3FeCl^+ = Ann + 3MgCl^+, \text{ etc.}$$

assuming that the solid phases and the fluid are in equilibrium with the melt. Oxygen fugacity was maintained through the equilibrium $Kfs + Mag = Ann + H_2$, and fluorine activity, through HF fugacity in fluid ($\log f_{HF} = 0.5$, see above). Thermodynamic data for the description of dissolved iron fluoride and chloride species were taken from the updated database of the SUPCRT 92 program (version of 1999). The calculated temperature dependency of iron and magnesium distribution between fluoride–chloride fluid and melt is shown in Fig. 13.

A series of computations in a wide range of oxygen fugacity (between the HM and QFM buffers) showed that Fe and Mg distribution is controlled mainly by temperature and concentrations of acids in the fluid and is independent of redox conditions. At high temperatures (>600°C), iron compounds (mainly, chlorides) are predominant in solution, whereas fluoride magnesium compounds are dominant below 550°C, when iron solubility is low (Fig. 13). Within the same temperature range, the concentrations of metal ions in fluid are high (10^{-3}–10^{-2} mol/kg), and their mass transfer by fluid can be significant (Haselton *et al.*, 1988; Borisov, 2000). These calculations probably have some bearing on the generation of high Fe/(Fe + Mg + Mn) HFSR through selective removal of magnesium from melts and metasomatic minerals at low near-solidus temperatures, i.e., during the process of their metasomatic transformation and subsequent melting. This suggestion is in agreement with the observed increase in Fe/(Fe + Mg + Mn) of both altered rocks and micas formed during HFSR degassing (Bacon, 1992; Abramov and Borisovskiĭ, 1996).

The behavior of metal solubility at varying temperature and f_{O_2} is qualitatively consistent with the experimental results of Whitney *et al.* (1985). These authors studied iron partitioning between silicic melt and aqueous chloride fluid. Their experiments revealed a maximum in iron solubility within a narrow temperature range of 600–550°C and lower iron contents at both higher and lower temperatures. It was also shown that iron solubility in fluid is independent of oxygen fugacity and is controlled by fluid salinity and temperature. These conclusions are in agreement with the results of our calculations.

Thus, the redistribution of Mg and Fe in the melt–fluid system is similar to the simulated REE behavior: fluid differentiation results in the extraction of the most soluble components from the magma. This process is efficient at the low temperatures of the beginning of melting of metasomatic assemblages in the channels transmitting fluids. With increasing temperature, the efficiency of fluid transport becomes negligible, and the compositions of magmas do not change any more.

CONCLUSIONS

The simulation of the process of fluid–magma interaction in silicic magmas reproduces the main characteristics of HFSR:

(1) existence of high-fluorine oxidized and reduced types of HFSR;

(2) active contacts of fluidized magmas with their wallrocks and magmatic replacement phenomena in consolidated granitoids at the contact with HFSR;

(3) formation of HFSR in the subvolcanic facies at low degrees of crystallization; and

(4) high Fe/(Fe + Mg + Mn) values and specific REE distribution patterns with similar chondrite-normalized contents of LREE and HREE and a strong negative Eu anomaly.

The obtained estimates of dynamic parameters allow us to propose scenarios for the development of fluid–magma systems.

The first stage is magma crystallization in the central parts of the intrusion and an increase in fluid pressure owing to retrograde boiling. In the central part of the intrusion, silicic magmas with 20–30% of crystals occur, and the crystallinity increases upward up to 100% at the temperature of roof rocks of 650–450°C.

The second stage includes steady-state fluid filtration under the established temperature gradient. As a result, magmatic mush (fluorine-rich melt + crystals) is formed within 2–500 y in the apical part of the intrusion. Bodies with vertical zoning are formed, and zones of metasomatized rocks develop in the frontal part of these bodies. Fluid filtration causes partial melting in the metasomatic rocks, and the generated melts show the strongest enrichment in fluorine and related components. The geochemical signature of HFSR is formed during this stage: flat REE distribution, melt depletion in LREE, Eu, and Mg and enrichment in HREE, Rb, Fe, and Mg. Depending on the relationships of temperature gradients and redox conditions in the magma source, either oxidized (f_{O_2} > NNO) or reduced (f_{O_2} < NNO) magmas are derived.

The third stage includes prolonged (5000–10000 y) fluid filtration, which results in the heating of the magma conduit to temperatures close to those of the central part of the intrusion. The efficiency of fluid

transport decreases with increasing temperature, and the compositions and geochemical signatures of magmas stop changing. As a result of the temperature increase, magmas in the channel conduit become liquid (with 10–20% of crystals). The completely liquid magma cannot transmit fluid (only heterophase systems are permeable). Thus, the passive degassing of the magma chamber ceases at this stage, and excess fluid pressure begins to rise. High fluorine contents and high temperatures strongly decrease magma viscosity. If the viscosity of these melts attains the critical value of fragmentation, catastrophic ejection of overheated magma may produce ignimbrites and topaz rhyolites. Another scenario implies the removal of high-temperature fluorine-rich melts into the subvolcanic level, where they form dikes, stocks, and small magmatic bodies. Which of the scenarios will be realized depends on the relationships between melt viscosity and excess fluid pressure (Wolff *et al.*, 1990; Mastin and Ghiorso, 2000).

The fourth stage must correspond to the end of the retrograde boiling process in the main chamber and, as a result, a decrease in temperature in the channel conduit. During this stage the main types of ore-bearing silicic magmas are formed (lithium–fluorine, geochemically normal, etc.), and their subsequent ore and geochemical features are defined. The transition from the progressive stage of melting front advance in the cupola to the regressive stage can probably occur at any moment during the evolution of the boiling system and is controlled only by processes in the main magma chamber (Syritso *et al.*, 2001). Such a multivariant character of transition between different stages of development is probably responsible for the diversity of silicic ore-bearing magma types.

ACKNOWLEDGMENTS

The author is grateful to N.N. Akinfiev (Moscow Geological Prospecting University) and K. Voletz (Los Alamos, USA), who provided programs for calculations and helped to apply them. A.V. Girnis, A.G. Gurbanov, A.V. Zotov, V.I. Kovalenko, A.M. Kurchavov, N.N. Pertsev, V.L. Rusinov, I.T. Rass, B.R. Tagirov (Institute of Geology of Ore Deposits, Petrography, Mineralogy, and Geochemistry, Russian Academy of Sciences), M.A. Korzhinskiĭ, L.I. Khodorevskaya, and K.I. Shmulovich (Institute of Experimental Mineralogy, Russian Academy of Sciences) are thanked for the discussion and constructive criticism of some concepts of the manuscript. The comments of S.P Korikovskii (Institute of Geology of Ore Deposits, Petrography, Mineralogy, and Geochemistry, Russian Academy of Sciences) substantially improved the style and clarity of presentation. This study was financially supported by the Russian Foundation for Basic Research, project nos. 99-05-65550, 01-05-64081, and 02-05-64904, and grant 311 for the support of young researchers of the Russian Academy of Sciences.

REFERENCES

1. A. M. Abdel-Rahman and R. F. Martin, Contrib. Mineral. Petrol. **104**, 173 (1990).
2. S. S. Abramov and S. E. Borisovskiĭ, Petrologiya **4**, 78 (1996) [Petrology **4**, 71 (1996)].
3. S. S. Abramov and A. V. Rasskazov, Geol. Rudn. Mestorozhd. **39**, 279 (1997) [Geol. Ore Deposits **39**, 237 (1997)].
4. S. S. Abramov, V. A. Kovalenker, and V. Yu. Prokof'ev, Vestn. Voronezh Gos. Univ., Ser. Geol., No. 11, 1 (2001).
5. S. S. Abramov, Dokl. Akad. Nauk **376**, 798 (2001) [Dokl. Earth Sci. **377**, 198 (2001)].
6. S. S. Abramov, Geokhimiya, No. 5, 1 (2000) [Geochem. Int., **38**, 464 (2000)].
7. J. J. Ague and G. H. Brimhall, Bull. Geol. Soc. Am., No. 6, 912 (1988).
8. N. N. Akinfiev, Geokhimiya, No. 6, 882 (1986).
9. A. M. Aksyuk and T. N. Zhukovskaya, Dokl. Akad. Nauk **361**, 240 (1998) [Dokl. Earth Sci. **361**, 745 (1998)].
10. N. F. Anikeeva, in *Some Problems of Petrography in Kazakhstan* (Moscow, 1968), pp. 34–49 [in Russian].
11. V. S. Antipin, E. A. Savina, and M. A. Mitichkin, Dokl. Akad. Nauk **357**, 531 (1997) [Dokl. Earth Sci. **357A**, 1346 (1997)].
12. C. R. Bacon, Trans. R. Soc. Edinburgh, Earth Sci. **83**, 27 (1992).
13. V. N. Balashov, G. P. Zaraĭskiĭ, and R. Seltmann, Petrologiya **8**, 563 (2000) [Petrology **8**, 505 (2000)].
14. S. M. Beskin, V. N. Larin, and Yu. B. Marin, *Associations of Rare-Metal Granitic Rocks* (Nedra, Moscow, 1979) [in Russian].
15. P. L. Blevin and B. W. Chappell, Trans. R. Soc. Edinburgh, Earth Sci. **83**, 305 (1992).
16. J. D. Blower, Bull. Volcanol. **63**, 497 (2001).
17. M. V. Borisov, *Geochemical and Thermodynamic Models of Hydrothermal Ore Formation* (Nauchnyĭ Mir, Moscow, 2000) [in Russian].
18. J. M. Brenan, Rev. Mineral., Contact Metamorphism **26**, 291 (1991).
19. S. V. Budnikov, Candidate's Dissertation in Geology and Mineralogy (Moscow, 1996).
20. D. M. Burt, M. F. Sheridan, J. V. Bikun, and E. H. Christiansen, Econ. Geol. **77**, 1818 (1982).
21. I. N. Bushlyakov and V. V. Kholodnov, *Halogens in the Genesis and Ore Potential of Granitic Rocks* (Nauka, Moscow, 1986) [in Russian].
22. N. G. Buzkova, *Studying of Rare-Metal Granitoids and Geologic Methods in Searches for Related Mineral Deposits* (Nedra, Leningrad, 1989) [in Russian].
23. Ph. A. Candela and Ph. L. Blevin, Econ. Geol. **90**, 2310 (1995).
24. Ph. A. Candela and P. M. Piccoli, in *Magmas, Fluids, and Ore Deposits, Mineral. Assoc. Canada Short Course* (1995), Vol. 23, pp. 101–126.
25. Ph. A. Candela, Trans. R. Soc. Edinburgh, Earth Sci. **83**, 317 (1992).
26. Ph. A. Candela, Am. Mineral. **76**, 1081 (1991).

27. Ph. A. Candela, Geochim. Cosmochim. Acta **50**, 1205 (1986b).
28. Ph. A. Candela, Chem. Geol. **57**, 289 (1986a).
29. S. S. Cardoso and A. W. Woods, Earth Planet. Sci. Lett. **168**, 301 (1999).
30. A. S. Chekhmir, A. G. Simakin, and M. B. Épel'baum, *Dynamic Phenomena in Fluid–Magma Systems* (Nauka, Moscow, 1991) [in Russian].
31. V. Yu. Chevychelov and M. B. Épel'baum, in *Contributions to Physicochemical Petrology* (Nauka, Moscow, 1985), Vol. 13, pp. 120-136 [in Russian].
32. V. Yu. Chevychelov, Geokhimiya, No. 5, 522 (1999) [Geochem. Int. **37**, 456 (1999)].
33. Yu. A. Chizmadzhev, V. S. Markin, M. R. Tarasevich, and Yu. G. Chirkov, *Macrokinetics of Processes in Porous Media* (Nauka, Moscow, 1971) [in Russian].
34. L. Chnagshi, H. Xiaolong, W. Rucheng, *et al.*, Chinese J. Geochem. **17**, 320 (1998).
35. E. H. Christiansen, J. V. Bikun, F. Sheridan, and D. M. Burt, Contrib. Mineral. Petrol. **83**, 340 (1983).
36. R. D. Congdon and W. P. Nash, Am. Mineral. **76**, 1261 (1991).
37. R. D. Congdon and W. P. Nash, Geology **16**, 1018 (1988).
38. R. E. Criss and H. P. Taylor, in *Rev. Mineralogy. Stable Isotopes in High-Temperature Geological Processes* (1986), Vol. 16, pp. 373–424.
39. G. R. Davies and A. N. Halliday, Geochim. Cosmochim. Acta **62**, 3561 (1998).
40. D. B. Dingwell, C. M. Scarfe, and D. J. Cronin, Amer. Mineral. **70**, 80 (1985).
41. V. S. Dmitrievskiĭ, Izv. Akad. Nauk SSSR, Ser. Geol., No. 3, 47 (1952).
42. W. A. Duffield and E. A. Du Bray, Am. Mineral. **75**, 1059 (1990).
43. J. C. Eichelberger, C. R. Carrigan, H. R. Westrich, and R. H. Price, Nature (London) **323**, 598 (1986).
44. A. J. Ellison and P. C. Hess, Geochim. Cosmochim. Acta **53**, 1965 (1989).
45. M. B. Épel'baum, in *Contributions to Physicochemical Petrology* (Moscow, 1978), pp. 179-183 [in Russian].
46. R. T. Flynn and C. W. Burnham, Geochim. Cosmochim. Acta **42**, 658 (1978).
47. B. R. Frost and D. H. Lindsley, in *Rev. Mineralogy. Oxide Minerals: Petrologic and Magnetic Significance* (1991), Vol. 25, pp. 433–462.
48. B. R. Frost, in *Rev. Mineralogy. Oxide Minerals: Petrologic and Magnetic Significance* (1991), Vol. 25, pp. 489–506.
49. C. D. Frost and B. R. Frost, Geology **25**, 647 (1997).
50. F. Gibert, D. Gullaume, and D. Laporte, Eur. J. Mineral. **10**, 1109 (1999).
51. C. M. Gramaccioli, V. Diella, and F. Demartini, Eur. J. Mineral. **11**, 983 (1999).
52. L. P. Gromet and L. T. Silver, Geochim. Cosmochim. Acta **47**, 925 (1983).
53. J. R. Haas, E. L. Shock, and D. C. Sassani, Geochim. Cosmochim. Acta **59**, 4329 (1995).
54. H. T. Haselton, Jr., G. L. Cygan, and W. D. D'Angelo, Econ. Geol. **83**, 163 (1988).
55. W. Hildreth, Geol. Soc. Am. Spec. Pap. **180**, 43 (1979).
56. J. P. Icenhower and D. London, Contrib. Mineral. Petrol. **127**, 17 (1997).
57. S. Ishihara, Mining Geol. **27**, 293 (1977).
58. G. F. Ivanova, G. M. Kolesov, and E. V. Cherkasova, Geokhimiya, No. 8, 1157 (1995).
59. J. W. Johnson, E. H. Oelkers, and H. C. Helgeson, Comp. Geosci. **18**, 899 (1992).
60. Yu. A. Kokotov and V. A. Pasechnik, *Equilibria and Kinetics of Ion Exchange* (Khimiya, Leningrad, 1970) [in Russian].
61. D. S. Korzhinskiĭ, Izv. Akad. Nauk SSSR, Ser. Geol., No. 12, 3 (1973).
62. V. P. Koval and V. Yu. Prokof'ev, Petrologiya **6**, 497 (1998) [Petrology **6**, 451 (1998)].
63. N. I. Kovalenko, *Experimental Study of the Genesis of Rare-Metal Li–F Granitoids* (Nauka, Moscow, 1979) [in Russian].
64. V. I. Kovalenko and N. I. Kovalenko, *Ongonites* (Nauka, Moscow, 1976) [in Russian].
65. V. I. Kovalenko and N. I. Kovalenko, in *Fluids in magmatic Processes* (Nauka, Moscow, 1982), pp. 121–137 [in Russian].
66. V. I. Kovalenko, N. V. Vladykin, E. V. Smirnova, and Yu. A. Balashov, Geokhimiya, No. 9, 1289 (1979).
67. V. I. Kovalenko, Yu. A. Kostitsyn, V. V. Yarmolyuk, *et al.*, Petrologiya **7**, 401 (1999) [Petrology **7**, 383 (1999)].
68. V. I. Kovalenko, V. B. Naumov, V. V. Yarmolyuk, and V. A. Dorofeeva, Petrologiya **8**, 586 (2000) [Petrology **8**, 525 (2000)].
69. A. M. Kutepov, A. D. Polyanin, Z. D. Zapryanov, *et al.*, *Chemical Hydrodynamics* (Byuro Kvantum, Moscow, 1996) [in Russian].
70. A. D. Kuznetsov and M. B. Épel'baum, *Eutectic Relations in Open Magmatic Systems with Perfectly Mobile Components* (Nauka, Moscow, 1985).
71. F. A. Letnikov, K. A. Kuznetsov, and V. Ya. Medvedev, Dokl. Akad. Nauk SSSR **313**, 682 (1990).
72. P. C. Lichtner, in *Rev. Mineralogy. Reactive Transport in Porous Media*, Ed. by P. C. Lichtner, C. I. Steefel, and E. H. Oelkers (1996), Vol. 34, pp. 1–79.
73. R. L. Linnen and A. E. Williams-Jones, Econ. Geol. **90**, 1148 (1995).
74. P. Lipman, M. Dungan, and O. Bachmann, Geology **25**, 915 (1997).
75. E. N. Lishnevskiĭ, Geol. Rudn. Mestorozhd., No. 5, 88 (1988).
76. E. N. Lishnevskiĭ, Dokl. Akad. Nauk **349**, 229 (1996) [Dokl. Earth Sci. **349**, 779 (1996)].
77. J. B. Lowenstern, Geology **22**, 893 (1994).
78. R. Macdonald, R. L. Smith, and J. E. Thomas, US Geol. Surv. Prof. Pap. **1523** (1992).
79. G. Mahood and W. Hildreth, Geochim. Cosmochim. Acta **47**, 11 (1983).
80. S. D. Malinin and I. F. Kravchuk, Geokhimiya, No. 8, 1110 (1995).
81. L.G. Mastin and M.S. Ghiorso, USGS Open-File Report **00-209** (2000).

82. V. K. Monich, *Petrology of Granitic Intrusions in the Bayanaul District, Central Kazakhstan* (Akad. Nauk Kaz. SSR, Alma-Ata, 1957) [in Russian].

83. G. Moore, T. Vennemann, and I. S. E. Carmichael, Geology **23**, 1099 (1995).

84. J. L. Munoz, in *Rev. Mineralogy. Micas* (1984), Vol. 13, pp. 469–493.

85. W. P. Nash, Am. Mineral. **78**, 1031 (1993).

86. V. B. Naumov, V. I. Kovalenko, and V. A. Dorofeeva, Geol. Rudn. Mestorozhd. **39**, 520 (1997) [Geol. Ore Deposits **39**, 451 (1997)].

87. V. B. Naumov, V. L. Rusinov, and V. A. Kovalenker, Dokl. Akad. Nauk **332**, 79 (1993).

88. E. V. Negrei, *Petrology of Upper Paleozoic Granitoids in Central Kazakhstan* (Nauka, Moscow, 1983).

89. D. C. Noble, W. L. Rigot, and H. R. Bowman, Geol. Soc. Am. Spec. Pap. **180**, 77 (1979).

90. E. H. Oelkers, in *Rev. Mineralogy. Reactive Transport in Porous Media*, Ed. by P. C. Lichtner, C. I. Steefel, and E. H. Oelkers (1996), Vol. 34, pp. 131–193.

91. V. G. Orlov, Geol. Rudn. Mestorozhd. **32**, 96 (1990).

92. A. R. Philpotts and M. Carroll, Geology **24**, 1029 (1996).

93. P. E. J. Pitfield, L. H. Teoh, and E. J. Cobbing, Geol. J. **25**, 419 (1990).

94. J. D. Price, J. P. Hogan, and M. Ch. Gilbert, Eur. J. Mineral. **8**, 435 (1996).

95. J. G. Price, S. B. Castor, and D. M. Miller, Am. Mineral. **77**, 1067 (1992).

96. A. Proussevitch and D. L. Sahagian, J. Geophys. Res. **101**, 17447 (1996).

97. A. H. Rankin, M. H. Ramsey, B. Coles, *et al.*, Geochim. Cosmochim. Acta, **56**, 67 (1992).

98. C. R. Rebbert, E. Partin, and D. A. Hewitt, Am. Mineral. **80**, 345 (1995).

99. M. Rieder, I. Haapala, and P. Povondra, Eur. J. Mineral. **8**, 593 (1996).

100. A. G. Rub, M. G. Rub, M. Shtemprok, and N. N. Krivoshchekov, Dokl. Akad. Nauk **367**, 402 (1999) [Dokl. Earth Sci. **367A**, 806 (1999)].

101. A. K. Rub and M. G. Rub, Izv. Akad. Nauk SSSR, No. 2, 42 (1991).

102. D. V. Rundkvist, V. K. Denisenko, and I. G. Pavlova, *Greisen-Related Mineral Deposits* (Nedra, Moscow, 1971) [in Russian].

103. I. D. Ryabchikov, N. A. Durasova, V. L. Barsukov, and A. S. Efimov, Geokhimiya, No. 6, 832 (1976).

104. G. N. Shcherba, *Genesis of Rare-Metal Deposits in Central Kazakhstan* (Akad. Nauk Kaz. SSR, Alma-Ata, 1960) [in Russian].

105. H. Shinohara and K. Kazahaya, in *Magmas, Fluids, and Ore Deposits. Mineralogical Association of Canada. Short Course Series* (1995), Vol. 23, pp. 47–70.

106. V. M. Shmonov, V. M. Vitovtova, and I. V. Zarubina, in *Permeability of Rocks at Elevated Temperatures and Pressures*, Ed. by K. I. Shmulovich, B. W. D. Yardley, and G. G. Gonchar (Chapman and Hall, London, 1994), pp. 285–313.

107. A. E. Silaev and V. V. Vasin, Zap. Vses. Mineral. O–va, Part CXVIII, 13 (1989).

108. A. G. Simakin and M. B. Épel'baum, in *Experimental and Theoretical Modeling of Mineral Formation* (Nauka, Moscow, 1998), pp. 56–71 [in Russian].

109. T. W. Sisson and C. R. Bacon, Geology **27**, 613 (1999).

110. R. S. J. Sparks, H. E. Huppert, and F. R. S. Turner, Phil. Trans. R. Soc. Lond. Ser. A. **310**, 511 (1984).

111. J. Stix and M. P. Gorton, J. Petrol. **31**, 1261 (1990).

112. J. Stix and G. D. Layne, J. Geophys. Res. **101**, 25181 (1996).

113. D. A. Sverjensky, Earth Planet. Sci. Lett. **67**, 70 (1984).

114. S. E. Swanson, J. F. Bond, and R. J. Newberry, Econ. Geol. **83**, 46 (1988).

115. L. F. Syritso, E. V. Tabuns, E. V. Volkova, *et al.*, Petrologiya **9**, 313 (2001) [Petrology **9**, 268 (2001)].

116. S. Tait, C. Jaupart, and S. Vergniolle, Earth Planet. Sci. Lett. **92**, 107 (1989).

117. V. L. Tauson, *Geochemical Types and Mineral Potential of Granitoids* (Nauka, Moscow, 1977) [in Russian].

118. B. E. Taylor, J. C. Eichelberger, and H. R. Westrich, Nature (London) **306**, 541 (1983).

119. G. M. Tsareva, V. B. Naumov, V. I. Kovalenko, *et al.*, Geokhimiya, No. 10, 1453 (1991).

120. J. D. Webster and W. A. Duffield, Econ. Geol. **89**, 840 (1994).

121. J. D. Webster, Contrib. Mineral. Petrol. **104**, 424 (1990).

122. H. R. Westrich, H. W. Stockman, and J. C. Eichelberger, J. Geophys. Res. **93**, 6503 (1988).

123. J. B. Whalen and B. W. Chappel, Am. Mineral. **73**, 281 (1988).

124. J. A. Whitney, J. J. Hemley, and F. Simon, Econ. Geol. **80**, 444 (1985).

125. J. H. Wittke, W. A. Duffield, and C. Jones, Am. Mineral. **81**, 135 (1996).

126. K. Wohletz and G. Heiken, *Volcanology and Geothermal Energy* (Univ. California, 1991).

127. J. A. Wolff, G. Wörner, and S. Blake, J. Volcanol. Geotherm. Res. **43**, 37 (1990).

128. G. P. Zaraiskii, Yu. B. Shapovalov, Yu. B. Soboleva, *et al., Physicochemical Parameters of Greisenization at the Akchatau Deposit: Geologic and Experimental Data* (Nauka, Moscow, 1994), pp. 371–419 [in Russian].

129. V. A. Zharikov, Vestn. Mosk. Gos. Univ., Ser. Geol. **4**, 3 (1996).